Renewable and Sustainable Energy Reviews 15 (2011) 169–185

Contents lists available at ScienceDirect

Renewable and Sustainable Energy Reviews

journal homepage: www.elsevier.com/locate/rser

# Segmented polymer electrolyte membrane fuel cells—A review

Luis C. Pérez [a], Lúcia Brandão [a], José M. Sousa [a,b], Adélio Mendes [a,*]

[a] LEPAE, Chemical Engineering Department, Faculty of Engineering, University of Porto, Rua Roberto Frias, 4200-465 Porto, Portugal
[b] Chemistry Department, University of Trás-os-Montes e Alto Douro, Apartado 202, 5001-911 Vila-Real Codex, Portugal

A R T I C L E   I N F O

*Article history:*
Received 1 August 2010
Accepted 6 August 2010

*Keywords:*
Polymer electrolyte membrane fuel cell
Direct methanol fuel cell
Segmented fuel cell
Current density distribution
*In situ* analytical techniques

A B S T R A C T

A complex interaction of many design, assembling and operating parameters as well as the properties of the materials used in the construction of polymer electrolyte membrane fuel cells (PEMFC) result in an uneven electrochemical performance over the MEA active area. For more than one decade, segmented PEMFC (SFC) have been used to study the factors responsible for that uneven performance. This paper reviews relevant literature related to SFC published since 1998 focusing on the three most important SFC design techniques: (1) printed circuit board, (2) resistors network and (3) Hall effect sensors. First, the three techniques are described and fundamental considerations for its design, construction and electrochemical characterization are provided. After that, the effect of most important parameters on the current density distribution is highlighted. Finally, representative results combining current density distribution measurements with other analytical techniques for distributed analysis are presented.
© 2010 Elsevier Ltd. All rights reserved.

**Contents**



* Corresponding author. Tel.: +351 22 508 1695; fax: +351 22 508 1449.
*E-mail address:* mendes@fe.up.pt (A. Mendes).

1364-0321/$ – see front matter © 2010 Elsevier Ltd. All rights reserved.
doi:10.1016/j.rser.2010.08.024

**Nomenclature**

| | |
|---|---|
| BP | bipolar plates |
| CC | current collectors |
| CDD | current density distribution |
| CNC | computerized numerical control |
| DAQ | data acquisition |
| DMFC | direct methanol fuel cells |
| EIS | electrochemical impedance spectroscopy |
| EOD | electro-osmotic drag |
| FRA | frequency response analyzer |
| GC | gas chromatography |
| GDL | gas diffusion layers |
| HFR | high frequency resistance |
| HTS | high temperature superconducting |
| LTS | low temperature superconducting |
| MEA | membrane–electrode assembly |
| NR | neutron radiography |
| OCV | open circuit voltage |
| ORR | oxygen reduction reaction |
| $P$ | pressure (bar) |
| PCB | printed circuit board |
| PEMFC | polymer electrolyte membrane fuel cells |
| $Q$ | volumetric flow rate (ml min$^{-1}$) |
| $RH$ | relative humidity (%) |
| SFC | segmented polymer electrolyte membrane fuel cells |
| SQUID | superconductive quantum interference devices |
| STR | self-draining stirred tank reactor |
| $T$ | temperature (°C) |

*Greek symbols*

| | |
|---|---|
| $\alpha$ | water transport coefficient (dimensionless) |
| $\lambda_{H_2}$ | stoichiometric ratio of hydrogen (dimensionless) |
| $\lambda_{air}$ | stoichiometric ratio of air (dimensionless) |
| $\lambda_{O_2}$ | stoichiometric ratio of oxygen (dimensionless) |
| $\rho$ | specific resistivity (m$\Omega$ cm$^{-1}$) |

*Subscripts*

| | |
|---|---|
| *air* | air from the atmosphere |
| *cell* | fuel cell |
| $H_2$ | hydrogen |
| *hum,a* | anode humidifier |
| *hum,c* | cathode humidifier |
| *met* | methanol |
| $O_2$ | oxygen |

## 1. Introduction

In order to accelerate the sluggish transition from R&D to full scale commercialization of polymer electrolyte membrane fuel cells (PEMFC) [1], efforts are still focused in overpassing delicate issues related to the hydrogen production and storage [2,3] and the development of hydrogen delivery infrastructures [4]. In the same way, recent publications highlight the need of cost reduction and further understanding of PEMFC systems regarding their degradation mechanisms and durability, water and thermal management, bipolar plates design and materials, catalyst load reduction and CO tolerance as well as the materials of the membrane–electrode assembly MEA [5–7]. To further understand PEMFC systems, a detailed analysis of the influence of main parameters on its performance and the development and combination of different *in situ* analytical methods is fundamental.

On the one hand, it is relatively well documented that PEMFC performance is affected by a complex interaction of many design, assembling and operating parameters as well as by the properties and microstructure of materials used on their construction. Design and assembling parameters include: (i) flow field geometry and (ii) clamping pressure. Operating parameters include: (i) species relative humidity, partial pressure and flow rate, (ii) temperature and (iii) total pressure. Finally, materials-related issues include: (i) properties and (ii) microstructure of materials, mainly at the MEA level. On the other hand, it has been pointed out by several authors that the most important implication of this complex interaction is an uneven electrochemical response of the MEA active area, the same that may lead to low reactants and electrocatalyst utilization, reducing the overall efficiency and accelerating aging [8–11].

In the last decade, segmented PEMFC (SFC) have proven to be an excellent *in situ* diagnostic tool to study the factors responsible for the uneven electrochemical response of the MEA active area. A SFC is similar to an ordinary fuel cell with the exception that one of the electrodes is divided into smaller electrodes, each of which can be interrogated for current, voltage and resistance, independently of the others [12]. In this work, the SFC definition embraces the PEMFC that permit the study of electrochemical phenomena (e.g. current, voltage or impedance) and/or monitoring different parameters (e.g. gaseous species composition, water accumulation or temperature) at a specific location of the MEA (a segment) so that a distributed performance analysis can be performed. Segmentation of a PEMFC involves accurate division of pertinent PEMFC components, namely the current collectors (CC), the bipolar plates (BP) or the gas diffusion layers (GDL). The distributed analysis and/or monitoring of different parameters is achieved with the individual characterization of the segments. Concerning the use of segmented and non-segmented PEMFC components, the different approaches proposed for SFC design, construction and electrochemical characterization can be divided in invasive, subdivided in three main categories, and non-invasive. The SFC classification adopted in this work is schematically shown in Fig. 1.

To the date, very few reviews described how SFC are used to perform discrete *in situ* electrochemical analysis [13] and physicochemical characterization [14]. Yuan et al. [13] analyzed the application of electrochemical impedance spectroscopy (EIS) to PEMFC research and highlighted the most representative works that perform local EIS measurements using SFC. Wu et al. [14] reviewed some approaches to measure local quantities such as temperature and current density. Wang [15] categorized the fundamental mathematical models that describe the physicochemical phenomena of PEMFC systems and stated that SFC can provide the experimental data required to validate them.

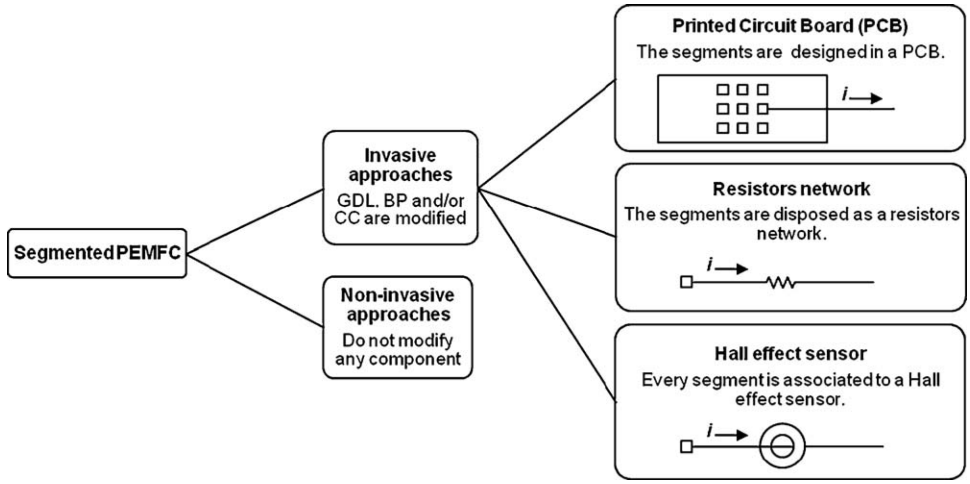



**Fig. 1.** Main approaches used for design, construction and electrochemical characterization of SFC.

This work targets: (i) providing fundamental understanding of the design and characterization techniques of SFC, (ii) to discuss the influence of the most important design, assembling, operating parameters as well as the materials properties on the current density distribution (CDD) of SFC and (iii) present the analytical techniques that have been combined with SFC since 1998.

## 2. Segmented PEMFC techniques

### 2.1. Main invasive approaches

The most frequently used invasive techniques for design, construction and electrochemical characterization of SFC can be classified into three categories: printed circuit board (PCB), resistors network and Hall effect sensors. These invasive techniques require segmentation of one or both of the following components: the CC, the BP and the GDL. There is no need to segment the membrane as it is ionically but not electrically connected to the GDL [16]. The three main techniques have been used at the German Aerospace Center (DLR) for both PEMFC and direct methanol fuel cells (DMFC) [1] characterization, a brief discussion of the advantages and disadvantages of each one was reported in Ref. [24]. It is noteworthy that SFC with different MEA active areas and number of segments have been studied using these techniques. The MEA active area is related to the power density of the cell while the number of segments is related to the resolution desired for the measurements. Small SFC with 1 $cm^2$ [17], 3 $cm^2$ [18], 5 $cm^2$ [19] and large with 370 $cm^2$ [9] and 578 $cm^2$ [20] MEA active area have been reported. The number of segments ranged between 3 [21] and 196 [22]. Table 1 summarizes the main characteristics of the SFC and the invasive technique used.

The strategies used to segment the fuel cell components are described in detail in Section 2.2, while some solutions to perform the local electrochemical measurements are given in Section 2.3. Fundamental considerations on design and electrochemical characterization of SFC are presented in Section 2.4. Below, the three most important invasive techniques are described in detail.

#### 2.1.1. Printed circuit board (PCB)

The PCB technique for electrochemical characterization of SFC was introduced by Cleghorn et al. [21]. The basic idea behind this technique is to replace one or both CC with a PCB. Using PCB manufacturing techniques, a segmented current collector can be designed on a thin, flat surface providing electrically isolated paths for individual current/voltage collection. The PCB is then placed between the flow field and the end plate, minimizing the local influence of the PCB on the thermal and electrical conductivity of the components while eliminating its interaction with the water evolution and transport inside the cell. The PCB substrates are epoxy-fiber glass [10,24] or polytetrafluoroethylene PTFE [25]. To facilitate the connection of the SFC to the measurement unit, the PCB can be plated-through-hole (PTH) [8,26]. The segments of the PCB are usually gold coated to avoid corrosion and minimize contact resistance. The reader is referred to Ref. [23] to deepen in PCB technology.

Interestingly, this technique offers the possibility to incorporate single straight [26], single [24] and multiple channel [8,10] serpentine flow fields directly on the PCB. With this, the functions of the flow field are integrated in the current collector; less components are needed to assembly the cell and the current is measured nearer the reaction site as the PCB is in direct contact with the GDL. These characteristics allow the insertion of the PCB between intermediate cells of PEMFC stacks [24]. In single cells,

**Table 1**
References of studies divided by active area, number of segments and SFC invasive technique.

| | Cell active are ($cm^2$) | | | | Number of segments | | |
|---|---|---|---|---|---|---|---|
| | 1–22.5 | 25–56 | 100–130 | 200–578 | 3–16 | 18–49 | 81–196 |
| Printed circuit board (PCB) | [11,18,19,26,61, 73,93,107,113] | [10,25,27,55,114] | [8,56,115] | | [19,26,27,55,56,61, 73,93,113,114] | [8,11,18,107,115] | [10,25] |
| Resistors network | [16,28,30,32,44, 45,50,51,60,80] | [29,33,36,48,49, 59,78,79,81,88, 94,96,98,100, 102,116,117] | [31,35,37] | [9,22,34, 58,86,103, 109,112] | [9,16,28,30,32,33, 35,37,45,49,50,51, 78,79,81,88,94,96, 98,102,103,109,112] | [29,31,34,36,44, 48,59,80,86,100, 116,117] | [22,58,60] |
| Hall effect sensors | | [46,47,52,53,74] | [12,54,92] | [20,21,40, 41,57,62, 75–77] | [12,21,40,41,46,47, 52,57,62,74–77,92] | [20,53] | [54] |

when one current collector is replaced by a PCB the other can remain unaltered so that the PCB can be placed between the anodic [8,27] or cathodic [10,26] bipolar plate and the end plate. When the PCB is placed at the anode, the cathode is available for complementary studies concerning water management [25]. The electrode where the PCB is placed does not affect significantly the CDD measurements [19]. An exploded view of a segmented fuel cell with a PCB of 100 segments incorporated as anodic current collector is shown in Fig. 2.

Company S++ (Germany) [111] offers three solutions for obtaining the CDD using the PCB technique: one oriented to large fuel cells and stacks, one with improved resolution capabilities (1152 segments) and the last with the flow fields incorporated directly on the PCB.

*2.1.2. Resistors network*

The principles of the resistors network technique were introduced by Stumper et al. [29] who developed two methodologies to measure the CDD in operating PEMFC. The first one, the subcells approach, consists of punching out several circular pieces of the GDL, replacing them with smaller, electrically isolated pieces with the same characteristics, the subcells. In this form, the current density could be measured independently at specific regions of the cell. The second methodology involves the use of a current mapping plate formed by 121 identical graphite cylinders equally distributed over a hexagonal area that matches the MEA active area. The graphite cylinders were packed and placed between the flow field and the end plate, creating a passive resistor network that assisted the CDD measurements.

Generically, in the resistors network approach, the anodic, the cathodic or both BP of a PEMFC is/are divided into electrically isolated segments of the same shape, forming a resistors network that incorporate a portion of the flow field. The electrochemical characterization of the SFC can then be made in two ways: passively or actively. The passive method involves the connection of a "precision", "high resolution" or "shunt" resistor in series with every resistor of the network so that the current density of each segment can be calculated from the voltage drop over the precision resistor. The nominal value of the precision resistors used in SFC characterization is 0.1 Ω [29–31], 0.012 Ω [32] or 0.01 Ω [33]. The resistors network can be arranged in a segmented current collector, permitting the use of unaltered BP and GDL [37]. A detailed explanation of the measurement principles for the passive method is given by Morimoto et al. [28]. Fig. 3 schematizes a segmented fuel cell using the resistors network technique and passive method for characterization. The segmented fuel cell has a segmented bipolar plate and gas diffusion layer at the anode and a precision resistor connected in series to each segment of the cell.

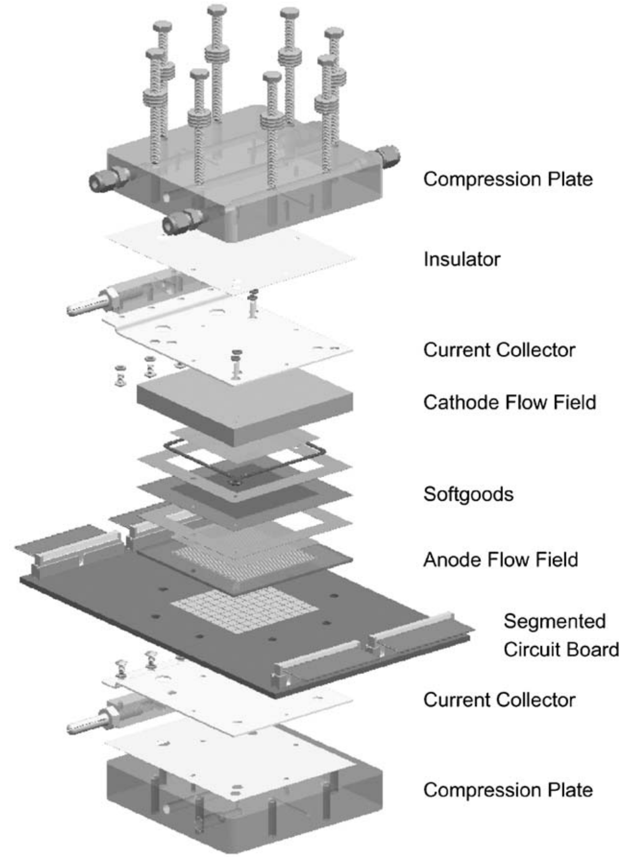



**Fig. 2.** Exploded view of a segmented fuel cell assembly using the PCB approach.From Ref. [25] with permission.

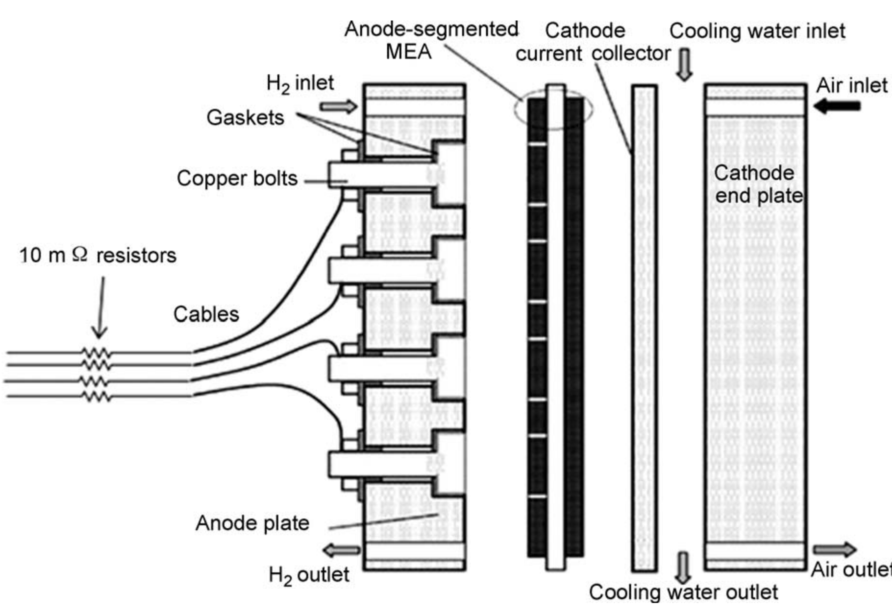



**Fig. 3.** Schematic of a segmented fuel cell using the resistors network approach and passive method for characterization.Adapted from Ref. [33] with permission.

The active method involves direct connection of the resistors network to the measurement unit, eliminating the use of the precision resistors [16,35,45,49,59,60]. In this case, the current flowing through each resistor of the network is read directly by the measurement unit.

Company Helmbold Messtechnik (Germany) [118] has developed a SFC with 196 segments and 244 $cm^2$ active area using a segmented graphite plate as cathode.

*2.1.3. Hall effect sensors*

The fundamentals of this technique were introduced by Wieser et al. [20]. This technique involves the association of one Hall effect sensor to every single electrically isolated segment of the segmented cell. A Hall effect sensor is a current transducer with four terminals: two for the connections to a source of current and two for the measurement of voltage across it [38]. Hall effect sensors work under the Hall effect principle, which states that when a current-carrying conductor is placed into a magnetic field, a voltage is generated perpendicular to both the current and the field [39]. When a Hall effect sensor is used in a segmented cell, the density of the magnetic flux passing through the Hall element determines the output voltage of the sensor, which is proportional to the current generated by the segment. Two Hall effect sensors topologies, namely open loop [12] and closed loop [40] have been used for SFC characterization. According to Geiger et al. [47] the closed loop Hall effect sensors are more accurate, more linear and easier to calibrate due to its lower sensitivity to changes in temperature. Interestingly, closed loop Hall effect sensors have been successfully used to measure the CDD at the outermost cells of a 3 cells PEMFC stack [41]. Fig. 4 schematizes the location of the Hall effect sensors integrated in the stack.

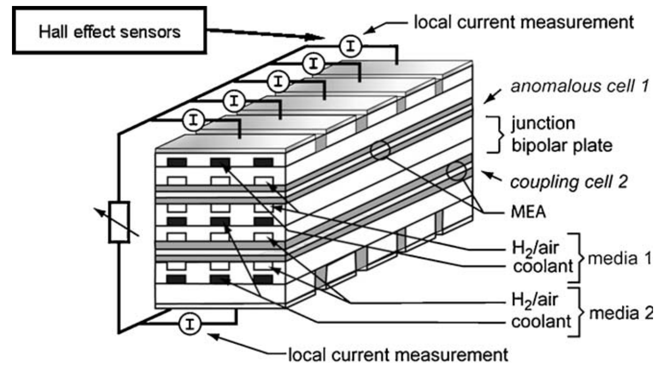



**Fig. 4.** Simplified scheme of a two-cell (1 + 1) stack with independent media supplies and location of Hall effect sensors at the stack periphery.Adapted from Ref. [41] with permission.

*2.2. Components segmentation*

Early efforts to modify pertinent components of PEMFC in order to obtain distributed electrochemical information were made by Rieke and Vanderborgh in the late-1980s [42]. Using modified photolithographic techniques, they created an array of microelectrodes placed directly on a perfluorosulfonic acid membrane in order to map the voltage and current distribution at the anode of a PEMFC. These authors highlighted for the first time the correlation between the spatially heterogeneous hydration of the membrane and the CDD. Another early work was presented by Vermeijlen et al. [43] who determined the potential distribution in an anodic gas diffusion layer made of carbon paper. These authors used 25 small electrical contacts mounted on a perforated acrylic (Perspex®) support that was pressed against the carbon paper. These authors computed the CDD along the carbon paper, concluding that the ohmic resistance of the carbon paper can play a major role in current and overpotential distribution of PEMFC.

More recent SFC designs incorporate different strategies to segment the GDL, the BP or the CC. The strategies presented below can help to design and construct SFC that use any of the three techniques previously introduced.

*2.2.1. GDL segmentation*

For SFC study, the GDL can be totally or partially segmented. With its partial or total segmentation, some authors have tried to minimize the electrical interaction between segments at the GDL level, so that more accurate measurements can be obtained. Total segmentation of the GDL is achieved by using silicone [9,12], Teflon® [8] or Teflon®/silicone [51] gaskets as a frame to accurately hot-press rectangular pieces of GDL over the membrane. A scheme of a totally segmented gas diffusion layer is presented in Fig. 5a. Hakenjos et al. [44] reported the only study using a partially segmented gas diffusion layer. It was prepared by cutting out 0.2 mm wide gaps from a Toray carbon paper gas diffusion layer, as seen in Fig. 5b. As a result, the ohmic resistance between adjacent segments increased up to 0.5 Ω.

*2.2.2. BP and CC segmentation*

Segmented BP suitable for SFC studies can be manufactured directly from a graphite block using computerized numerical control techniques (CNC) and a bonding agent, which is usually an epoxy resin that provides good electrical insulation and mechanical stability [27,46]. The manufacturing process involves the following steps [27,46]: (1) the segments are partially milled, (2) the gaps are filled with resin, (3) once the resin is cured, the opposite face of the plate is milled so the segments are electrically isolated, (4) both sides of the BP are polished and (5) the flow field is machined. The most important manufacturing steps are schematically illustrated in Fig. 6 for a bipolar plate with 9

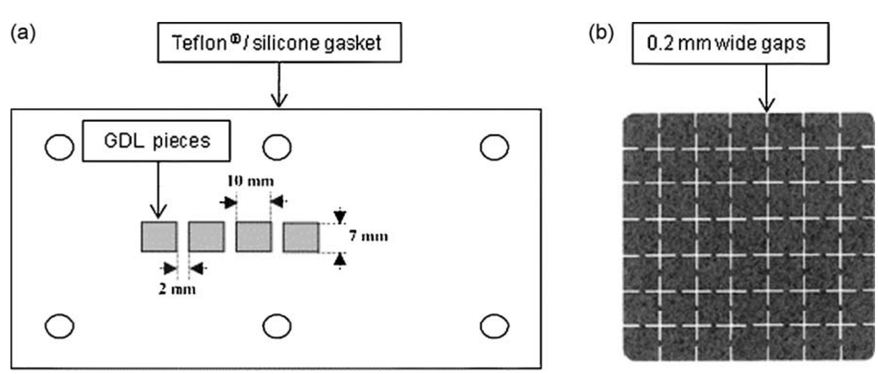



**Fig. 5.** (a) Scheme of a totally and (b) picture of partially segmented GDL for use in SFC.From Ref. [51] (left) and [44] (right) with permission.

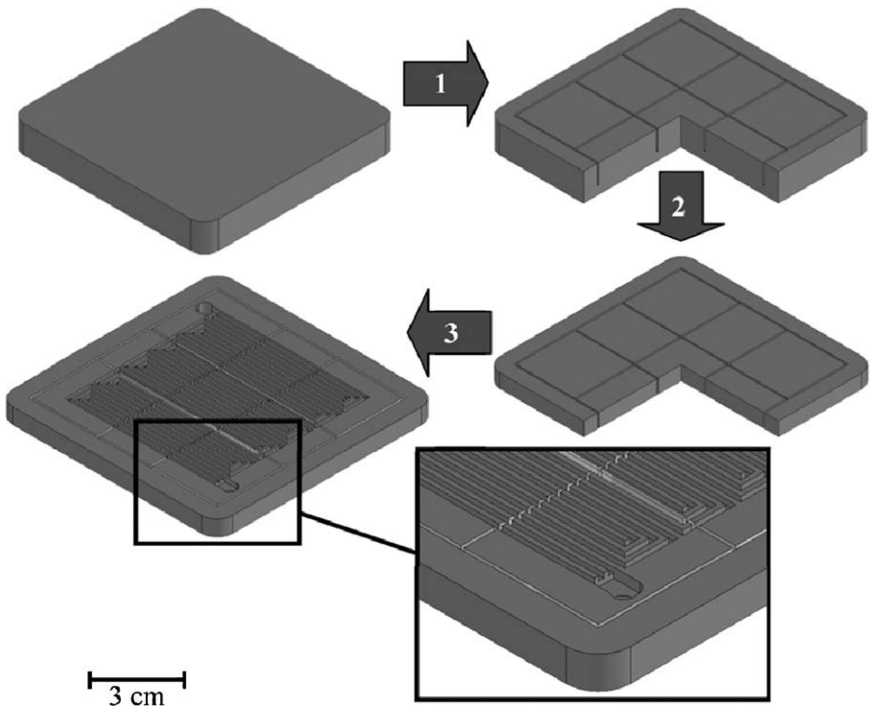



**Fig. 6.** Illustration of the manufacturing process of a segmented flow field plate made of graphite.From Ref. [27] with permission.

segments. A similar strategy was presented by Geiger et al. [47] who first glued three graphite bars with a two-component epoxy adhesive. After the epoxy adhesive was cured, the glued plate was milled perpendicular to the bonding surface and reunited following the same procedure as before. Finally, the flow field was machined.

The BP can also be segmented by embedding conductive prism-shaped blocks, normally quadrangular, into a non-conductive polymeric frame. After that, the flow field can be machined. A picture of a segmented bipolar plate with 16 titanium-coated stainless steel blocks (segments) inserted in a polyoxymethylene frame is schematically shown in Fig. 7. Non-conductive materials used as frames include polysulfone [18,35,48], polycarbonate [30,31,49,50], acrylic [9,51], polyoxymethylene [52], polyetherimide [12], poly(methyl methacrylate) [53], bakelite [54] and organic glass [40]. Conductive materials embedded in the polymeric frames are copper [35,37], graphite [9,12,18,40,48,49,51,54] and stainless steel [30,50,52]. In order to prevent corrosion and reduce contact resistance, the conductive prism-shaped blocks are usually coated with gold [35,37,49] or titanium [52]. Direct current collection from these embedded prisms is then obtained by attaching copper wires [30,35], gold wires [53], silver-coated copper sticks [40], stainless steel pins [50] and copper blocks [54] to the conductive prisms. Alternatively, copper bolts can be inserted in a block of the same material and then electrically isolated using plastic gaskets [33]. To prevent reactants leakage, epoxy [12,52] and bakelite resins [54] can be used.

The integration of segmented BP with similar characteristics than the ones used in real stacks has also been reported. Büchi et al. [57] developed the so-called semi-segmented plate concept. The plate consists of three elements: (i) a pressure molded flow field made of a graphite–polymer mixture with high specific resistivity ($\rho \approx 25\ \mathrm{m\Omega\ cm^{-1}}$), (ii) highly conductive segments of sintered graphite glued to the flow field with $\rho \approx 1\ \mathrm{m\Omega\ cm^{-1}}$) and (iii) individual metal current collectors. The semi-segmented plate has the same electrical, fluid dynamic

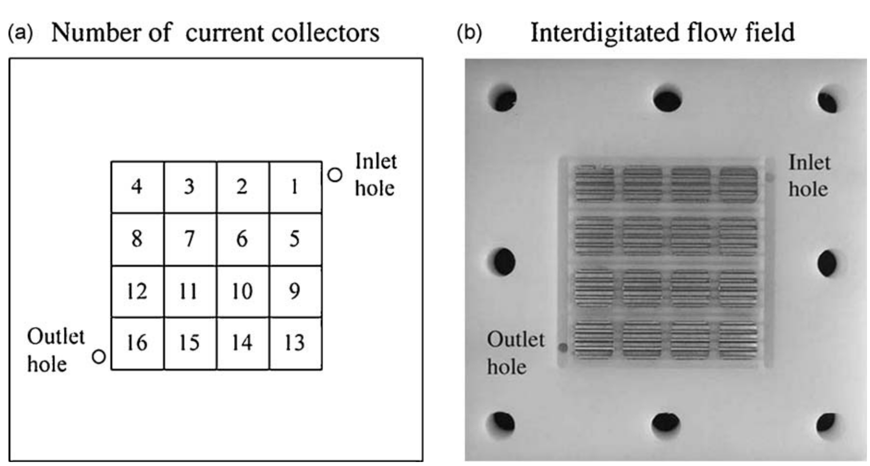



**Fig. 7.** To the left, location of the current collection segments. To the right, segmented bipolar plate fabricated by inserting conductive prism-shaped blocks (silver gray blocks) into a non-conductive polymeric frame (in white).From Ref. [52] with permission.

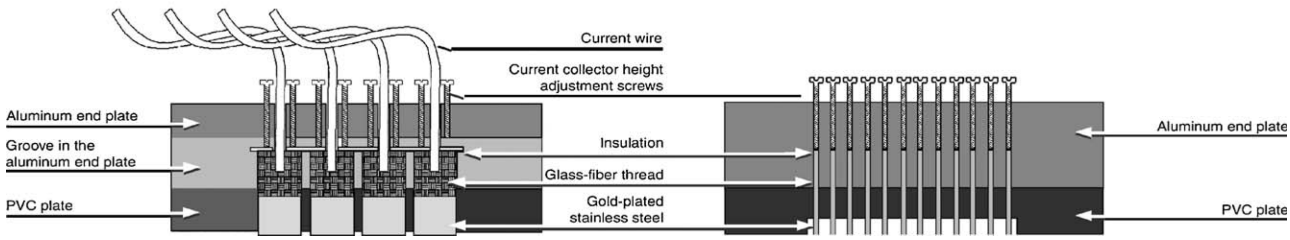



**Fig. 8.** Cross-sections from the segmented cathode flow-field plate. The left one is the vertical and the right one is the horizontal cut.From Ref. [29] with permission.

and thermal properties as the BP used in PEMFC stacks with up to 125 cells.

An interesting contribution was made by Ghosh et al. [34] who refined the current mapping plate concept. The plate was made of expanded graphite with 20 segments and isolated copper wires attached for current collection. In turn, the plate was sandwiched between two semi-segmented and two unaltered plates, forming a five-layer CDD measuring device with a thickness of 3 mm that can be integrated in PEMFC stacks.

It is noteworthy that Noponen et al. [29] incorporated a segmented current collector in a free breathing PEMFC. In a free-breathing or open cathode PEMFC, natural convection is the driving force for oxidant distribution along the cathode GDL as it is open to the atmosphere. A polyvinyl chloride (PVC) block served as electrical insulator of the 48 cathode gold-plated stainless steel current collectors. Every current collector (positioned orthogonally to the end plate surface) had a screw to adjust height and assure good electrical contact with the GDL. An aluminum endplate was attached to the PVC block to provide mechanical stability. Fig. 8 shows details of this segmented current collector.

### 2.3. Local current/voltage measurement

To obtain relevant electrochemical information of a segmented cell it is important to measure the current, voltage, high frequency resistance (HFR) and/or electrochemical impedance spectroscopy (EIS) of each segment. It is important to mention the efforts made by some research groups aiming to compensate the voltage drop across the segments when using the PCB and the resistors network approach for CDD measurements.

Kulikovsky et al. [18] plugged the PCB of their SFC to a measurement unit that incorporates a shunt resistor and an amplifier to convert the current into a voltage signal. The unit included a circuit for voltage drop compensation across the PCB paths and shunt resistor, providing in this way equal potential to all segments. A system for active voltage drop compensation using a PCB was developed by Sauer et al. [11]. The system included the connection of the segments to a voltage source and a transistor in series with a shunt resistor. Santiago et al. [27] proposed another solution to measure the current and voltage in a PCB with voltage drop compensation. Each path of the PCB permitted the connection of the segments to individual low impedance (0.18 m$\Omega$) closed loop Hall effect sensors. The current measured by the Hall effect sensors was then converted to a potential by connecting the former to individual precision resistors of 1 k$\Omega$.

Concerning the resistors network technique, Siroma et al. [60] reported the use of a data logger and a 100 channel zero-shunt current/voltage converter to obtain the current and minimize voltage drop through the segments. Tabe et al. [31] reported another strategy, these authors connected variable resistances to each segment, so that their individual resistance could be calibrated and the difference in contact resistance compensated. At the beginning of the experiments, the overall cell resistance was set to a constant value by adjusting the variable resistances in order to obtain a uniform CDD of 0.5 A cm$^{-2}$.

The use of Hall effect sensors facilitates the measurement of the CDD, being necessary only a data acquisition (DAQ) unit and a multiplexer as done by Wieser et al. [20] and Geiger et al. [47].

Complementarily, HFR and EIS measurements can be performed with in-house built measurement systems [46] or commercial frequency response analyzer (FRA) [8,12,32,61]. Companies Zahner-elektrik GmbH & Co. KG (Germany) and Arbin Instruments (USA) offer multichannel potentiostats/galvanostats to perform both CDD and EIS measurements.

### 2.4. Fundamental considerations for SFC design

#### 2.4.1. Components

In this section, general recommendations for segmentation of the components are given. First of all, it should be noted that GDL segmentation requires BP and CC segmentation, increasing the complexity of the design and its assembly [40,49]. To overcome this, partial segmentation of the GDL is a fair option as it reduces electrical interaction between segments and is not as time demanding as total segmentation. Total segmentation of the GDL can lead to misalignment problems between corresponding anodic and cathodic parts of the GDL the same that can lead to membrane failure due to thinning via chemical degradation and pinhole formation [104].

If the BP are segmented, they must provide uniform and robust mechanical support to the MEA, otherwise the MEA can break down at high current densities (≈1 A cm$^{-2}$) from the places with poor mechanical support [59]. Gas leakages may appear if segmented the BP are constructed by inserting conductive prisms into a non-conductive polymer frame. The use of epoxy resins is a common practice as it prevents gas leakages and glues the prisms to the frame. It is very important to reduce the electrical resistances of metallic surfaces by coating them with titanium, silver or gold; another option is to insert graphitic foils between them.

It is important to keep the pressure distribution between components as uniform as possible or the segments will have different contact resistances, affecting the measurements. The pressure distribution between surfaces can be checked with pressure sensitive films [12,36] while uneven contact resistance can be corrected by connecting a variable resistance to every segment as stated above. More sophisticated ways to evaluate the contact resistance variations between segments involve measuring the HFR each segment at two different relative humidity (RH) conditions with the SFC running on air at the anode and the cathode [53] or using the four wire resistance measurement method to determine their impedance [27].

Regarding the wiring array used to connect the cell to the measurement unit, it must be kept as short as possible to reduce ohmic losses [19].

#### 2.4.2. Uncertainties associated to the use of SFC

There are uncertainties related to structural differences between SFC and regular PEMFC. The evaluation of these

uncertainties has served to validate the use of SFC as analytical technique and has been focused on two aspects: (i) the need of GDL and BP segmentation and (ii) the relative error introduced by the auxiliary measurement circuitry system of SFC.

The discussion around the need of GDL and BP segmentation has been focused on how the in-plane and through-plane electrical conductivity of components (i.e. the use of non-segmented GDL along with segmented BP) affect the local electrochemical characterization of the segments. Researchers have evaluated the need of the GDL or the BP segmentation both numerically and experimentally. All the mathematical models used to evaluate numerically the uncertainties aimed to simulate the solid phase potential distribution in repetitive current-collecting elements at different current densities [29,51,56].

For example, Noponen et al. [29] used 48 electrically isolated pins in direct contact with a non-segmented GDL for direct current collection and observed a difference in performance no greater than 10% between adjacent segments at different experimental conditions. These authors also simulated the effect of using a non-segmented GDL on the current collection of four neighboring segments using the FEMLAB® multiphysics software package. From the simulations, they concluded that current density from each segment can be measured with reasonable accuracy even if the GDL is not segmented as far as the contact resistance differences between the segments and the GDL are minimized. Natarajan and Nguyen [51] evaluated the effect of GDL segmentation in a different form. These authors obtained galvanostatic and potentiostatic polarization curves for each segment using segmented BP and CC. Segmented and non-segmented GDL were used in the MEA and the results were compared. For both segmented and non-segmented GDL, differences in segment performance were minimal in the galvanostatic tests. The potentiostatic tests showed a minimal difference in performance for each segment when using a segmented GDL. For the non-segmented GDL, on the other hand, the potentiostatic tests showed a significant difference in performance for each segment. Overall cell performances were similar, irrespective of the type of test, potentiostatic or galvanostatic. Finally, it was recommended: (i) to segment the GDL along with the BP and the CC as contact resistance variations between the BP and the GDL are negligible, irrespective of the type of test and (ii) to perform galvanostatic tests rather than potentiostatic tests if the GDL is non-segmented, as this minimizes differences for each segment performance due to uneven electrical contact resistances between the segments and the GDL.

The need of BP segmentation was discussed by Eckl et al. [56], who evaluated the effect of BP segmentation using a segmented anodic bipolar plate with resistors network and a non-segmented anodic bipolar plate with a PCB as current collector. The cathodic bipolar plate and current collector as well as the GDL remained unaltered in both cases. For the resistors network case, the major parameters causing lateral current spreading (from segment to segment) were found to be the resistance difference of the individual measurement circuits and the current density gradient between neighboring segments. Due to non-segmentation of the bipolar plate, the PCB showed higher lateral current spreading; however, it was proposed by these authors that the use of a PCB along with non-segmented BP provide a good alternative for CDD measurements.

The error introduced by the auxiliary measurement circuitry has been evaluated individually for each approach and concerns the use of PCB, resistors network and Hall effect sensors. Regarding the use of PCB, Sauer et al. [11] used an empirical formula to calculate the relative error in current measurements introduced by their PCB with active voltage drop compensation. The cell was operated galvanostatically; it had a non-segmented GDL and segmented anodic bipolar plate and current collector. The relative error of the current measurement was less than 6.5%. Concerning the use of precision resistors, Noponen et al. [59] and Liu et al. [33] used non-segmented and segmented GDL, respectively. In both studies, only the anodic flow field and current collector were segmented. Relative errors in the range 1–2% were found in both cases. With respect to Hall effect sensors, Wieser et al. [20] used a segmented anodic and a regular cathodic bipolar plate. The GDL remained unaltered. After measuring the lateral currents at the GDL, they computed a relative error below 5% for the current gradient between neighboring segments. Due to calibration of the Hall effect sensors used, Geiger et al. [47] and Santis [62] reported relative errors within 1% and between 0.5 and 0.17%, respectively.

### 2.5. Other invasive approaches

This section describes how the local electrochemical behavior of operating PEMFC can be studied using different segmentation strategies and analytical techniques than the ones listed before. Sun et al. [68] developed the so-called current measurement gasket technique. The gasket was fabricated of an epoxy resin and glass cloth substrate. On one side of the gasket, 23 gold-plated copper rectangles were outlined in such a way that those surfaces matched exactly the 23 single channel flow field ribs of the cathode. Once assembled, the current collection portions were in direct contact with the cathodic gas diffusion layer. Both the anodic and cathodic BP suffered no modifications. The gasket adapted for CDD measurements is shown in Fig. 9.

Some research groups have focused on increasing the resolution of CDD measurements. A methodology to measure the current under the gas channel and under the rib of a flow field was reported by Wang and Liu [67]. Three MEA with a regular anode and a differently arranged cathode were assembled. The first cathodic GDL was loaded with catalyst only at the regions above the gas channels, the second was loaded at the region above the single rib and the third was fully covered with catalyst. The resolution of measurements was further increased by Freunberger et al. [17] and Büchi and Reum [65] from the Paul Scherrer Institute. These authors reported local current density and local membrane resistance measurements with sub-millimeter resolution using a laboratory PEMFC with 1.3 $cm^2$ active area. The measurement methodology is explained in a report by Freunberger et al. [66].

The indirect determination of the CDD has been achieved in different ways. Wilkinson et al. [69] calculated the CDD along the channel of a Ballard Mk V single PEMFC from local temperature

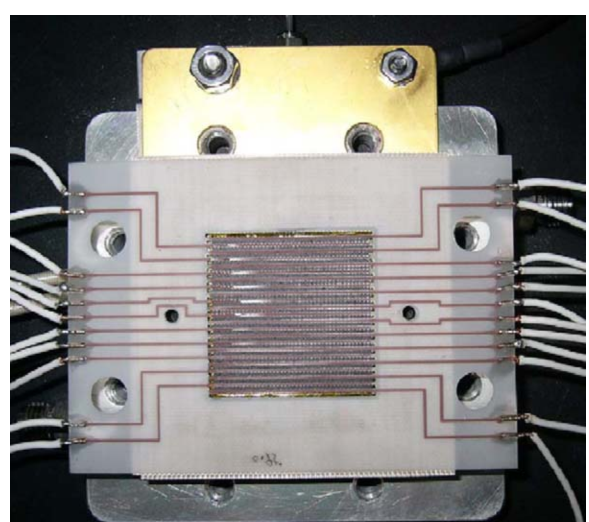


**Fig. 9.** Picture showing the location of the current distribution measurement gasket.From Ref. [68] with permission.

distribution measurements. Seventeen K-type thermocouples of 0.254 mm diameter were embedded in different locations of the anode flow field. Heat generation due to the exothermic reaction of hydrogen oxidation was correlated to the temperature of each thermocouple. Another way to indirectly estimate the CDD was reported by Araki et al. [32]. These authors used a gas chromatograph (GC) to measure the gas composition of reactants along a cathode with eight gas sampling ports. The CDD was calculated from the decreased flow rate of $H_2$ and $O_2$ along the flow field. Alternatively, Candusso et al. [63] and Sailler et al. [64] used one-axe and two-axe sensitive magnetic field sensors, respectively, to measure the instantaneous magnetic field as close as possible to the MEA. The CDD was then calculated using the Maxwell's equations.

### 2.6. Non-invasive approaches

The non-invasive approaches for local electrochemical characterization of operating PEMFC present the particularity that no physical modifications are made to any of the components involved in the fuel cell assembly. Non-invasive techniques are supported by sophisticated magnetic field measurement devices. Claycomb et al. [70] employed high temperature superconducting (HTS) and low temperature superconducting (LTS), superconductive quantum interference devices (SQUID) and flux gate magnetometers to obtain spatial magnetic field maps of an operating PEMFC. SQUID are magnetic flux-to-voltage transducers often used in non-destructive and non-invasive analysis of materials [71]. Hauer et al. [72] introduced a magnetic inducted tomography technique to indirectly measure the CDD. Two 3D magnetic field sensors were used for the readings. One sensor scanned the upper while the other scanned the lower part of the cell. The experimental set-up allowed four-axis scan measurements, creating a CDD map of the fuel cell.

## 3. Parameters influence on current density distribution

The simplest way to study the distributed electrochemical performance over the MEA active area is to measure the CDD. In this section, the effect of relevant design, assembling and operating parameters as well as the use of different MEA materials on CDD is discussed. To analyze the effect of one parameter, researchers have kept constant the others. Table 2 summarizes the parameters studied using SFC.

The CDD profiles have been graphically presented in several forms, for example: as a surface on which the current density is represented as discrete sections of the MEA active area [54,55,86], as a trend line on which the current density is presented as a function of the fractional distance from the inlet of the cell [109,113] and as a trend line on which the current density is presented as a function of every segment of the cell [33,48,75].

Despite its importance, few authors have developed strategies for homogenizing the CDD. Santis et al. [119] tried to achieve this goal by using cathodic GDL with different Pt catalyst loading gradients along the air flow field channels. The anodic and cathodic GDL had an average Pt loading of 0.6 mg $cm^{-2}$. Below, the effect of each parameter on the CDD is discussed in detail.

### 3.1. Flow field geometry

In a PEMFC, the flow field geometry determines how the reactants are distributed over the MEA active area. So far, the flow fields considered in SFC studies have been: single and multiple channels serpentine flow fields [8,34,36,49,54,55]; straight single and multiple (parallel) channels flow fields [18,25,26,48,50,53]; flow fields with net/grid geometry [59,96], interdigitated flow fields [95], self-draining stirred tank reactor (STR) flow fields [80] and biomimic flow fields [52].

Several research groups have aimed to compare different flow field geometries using CDD profiles. Hogarth et al. [80] compared two cathodic flow fields, a single channel serpentine and an STR. The anodic flow field had a net/grid geometry in both cases. The comparison was done under three low humidity conditions, the first with the anode humidifier temperature ($T_{hum,a}$) equal to the cathode humidifier temperature ($T_{hum,c}$) at 30 °C, the second with $T_{hum,a} = T_{hum,c}$ = 10 °C and the third dry. The temperature of the fuel cell ($T_{cell}$) ranged from 75 to 85 °C. The stoichiometric ratio of hydrogen ($\lambda_{H_2}$) ranged from 1.2 to 4.6 and the stoichiometric ratio of air ($\lambda_{air}$) ranged from 1.9 to 3.3. The STR showed improved overall performance at both the highest (5–10% improvement) and the lowest (∼25% improvement) RH conditions. Both tests showed higher current densities towards the outlet, nevertheless the single channel serpentine flow field showed very low activity at the cathode inlet in the dry condition. Recently, Hwnag et al. [52] evaluated four different cathodic flow fields namely a parallel, a multiple channels serpentine, an interdigitated and a biomimic (square-wave geometry) using CDD measurements. At the anode, a multiple channels serpentine flow field was used. The cell was operated at different conditions: 40 °C ≤ $T_{cell}$ ≤ 60 °C, $T_{hum,a}$ = 40 °C, $\lambda_{H_2} = 1.5$, 40 °C ≤ $T_{hum,c}$ ≤ 70 °C and $2.5 \leq \lambda_{O_2} \leq 3.5$. The CDD was tracked for 45 min. Due to superior mass transfer (diffusion) and water removal capabilities, the multiple channels serpentine flow field showed the most steadily CDD and the highest power density among the cathodic flow fields tested. The comparison of the parallel and the multiple channels serpentine flow field is shown in Fig. 10.

Hiseh et al. [19] developed a comparative study involving interdigitated, multiple channels serpentine, parallel and net/grid geometry flow fields while Zhang et al. [97] compared interdigitated and single channel serpentine flow fields. In both studies the anode and cathode had equal flow field geometries during the CDD measurements. These authors observed a more uniform CDD

**Table 2**
References analyzing parameters that influence the current density distribution using SFC.

| Parameter | References |
|---|---|
| Design/assembling | |
| Flow field geometry | [19,31,52,59,80,96,97] |
| Clamping pressure | [9,20,31] |
| Operating | |
| Reactants relative humidity | [8–10,21,25,28,33,37,45,49,50,52,54,57,59,73,77,79,81,86,102,103,113,117] |
| Reactants flow rate | [8,21,22,28,30–36,40,41,44–46,48,49,52,53,57,59,73,75–77,79,86,88,91,98,100,109,116,117,120] |
| Operating pressure | [33,34,67,68,85,86,88] |
| Contaminant species (CO, $CO_2$ and $NO_2$) | [40,58,92–94,112,114] |
| Materials | |
| Membrane thickness | [49,55] |
| GDL macrostructure | [10,51,81] |
| Permeability of the membrane to methanol | [91] |

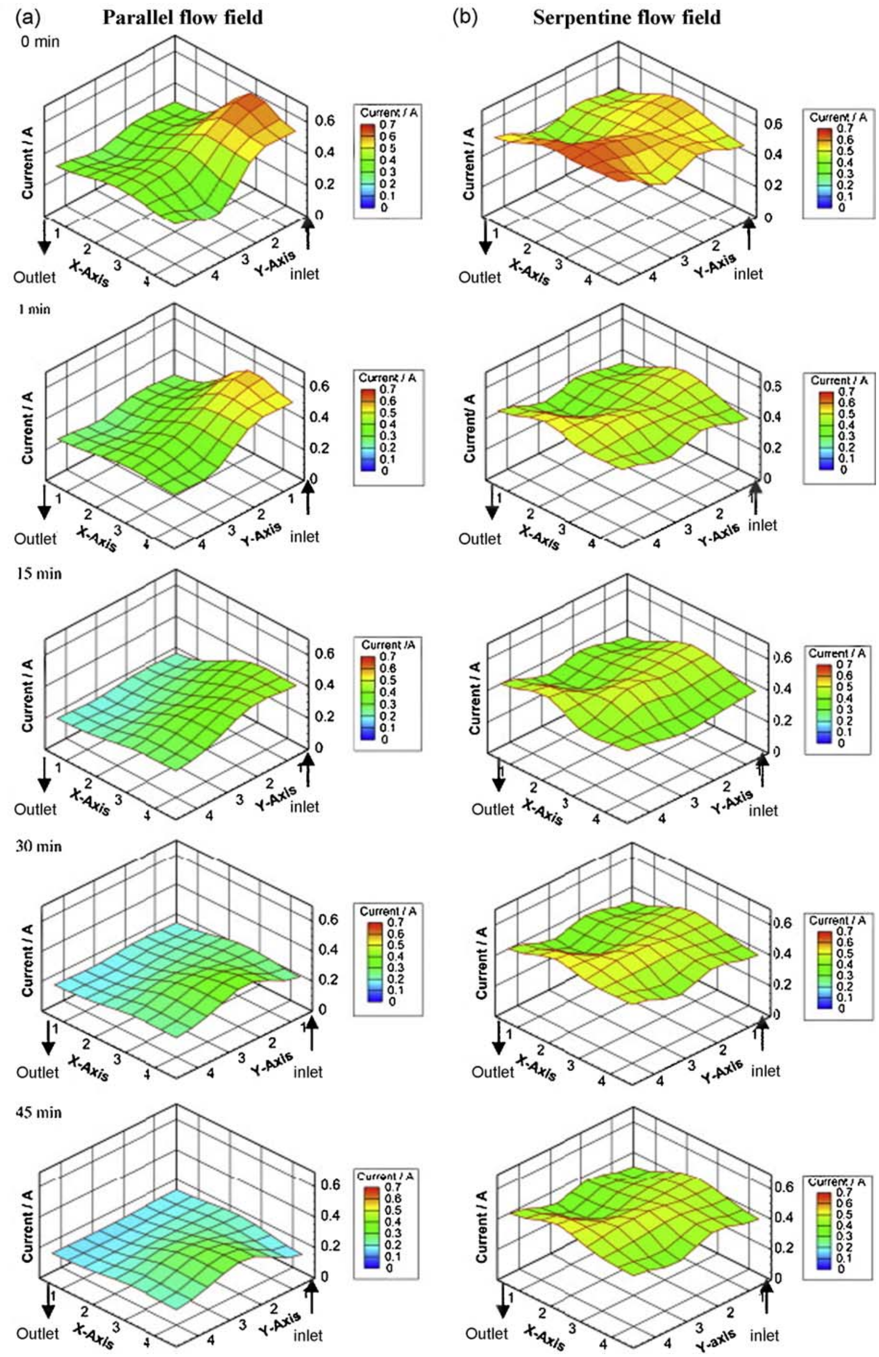



**Fig. 10.** Transient developments of the local current distribution, (a) parallel flow field and (b) serpentine flow field, $U$ = 0.5 V, $T_{cell}$ = 40 °C, $\lambda_{H_2} = 1.5$ and $\lambda_{O_2} = 2.5$.From Ref. [52] with permission.

profile for transient ($0\,h < t < 3\,h$) [19] and steady-state [97] operation when using the interdigitated flow field on both electrodes. The last was attributed to the convection-driven mass transfer mechanism of the reactants in this type of flow fields.

The effect of most relevant flow field geometric parameters (e.g. channel/rib width) on CDD was investigated by Reum et al. [110]. Several channel/rib configurations were used in their SFC with increased CDD measurement resolution. It was concluded that a flow field design with wider ribs and smaller channels can lead to higher and more homogeneous performances for a wide range of operating conditions (oxygen fractions above 10%) due to improved water management.

It is accepted that, on a general basis, more uniform CDD profiles are observed when reactants are fed in counter flow mode, that is, when the fuel and oxidant inlet and outlet are located at opposite sites [28,30,46,98].

Concerning DMFC, Gülzow et al. [96] compared a net/grid and a single channel serpentine flow field placed at the cathode. A net/grid flow field was used at the anode in both cases. The methanol flow rate ($Q_{met}$) was 20 ml min$^{-1}$ and had a 1.5 M methanol concentration while the air flow rate ($Q_{air}$) was 600 ml min$^{-1}$, dry. The anode and cathode pressure was 2.5 and 3.5 bar, respectively, and $T_{cell}$ = 90 °C. The CDD profile for the serpentine flow field was more homogeneous and showed a low current density zone near the cathode inlet associated to the drying effect of air on the membrane. The net/grid flow field showed high activity at center while the corners were producing almost no current.

### 3.2. Clamping pressure

In PEMFC systems, the clamping pressure is related to the tightening torque applied to the bolts located at the endplates. The clamping pressure is equal to the force required to compress the MEA, gaskets, BP and CC so that the pressure between these components is as uniformly distributed as possible and the PEMFC is gas tight. Due to differences in design and materials, every PEMFC system has its own clamping pressure. Using SFC, few groups have investigated the effect of clamping pressure on CDD; nonetheless, this is a parameter that must be taken into account when assembling a single cell or stack. Indeed, a recent study [99] reported that the local mass, charge and heat transfer properties of the GDL can vary significantly due to inhomogeneous compression caused by the flow field geometry of the BP over the MEA. Tabe et al. [31] analyzed how two different clamping pressures (0.6 and 1.2 MPa) affected the CDD at $T_{hum,a} = T_{hum,c} = 40\,^{\circ}C$ and $T_{cell} = 50\,^{\circ}C$ and for $\lambda_{H_2} = 1.3$ and $\lambda_{O_2} = 1.4$. The CDD was measured 240 s after starting the experiments. The CDD was higher for 0.6 MPa because of the lower mass transfer resistance of the GDL. On the other hand, the higher clamping pressure exhibited a more uniform CDD due to a more uniform contact pressure between the GDL and the BP.

### 3.3. Relative humidity of reactants

In technical fuel cells, gradients in reactant RH are unavoidable along the flow fields [82]. The RH of reactants plays a key role in keeping a correct level of hydration of the membrane and strongly influences the water transport mechanisms, namely the electro-osmotic drag (from anode to cathode) and the back-diffusion (from cathode to anode) of water [83]. Generally, as reactants are fed at lower saturation states, the membrane will not achieve a good hydration level near the inlet, increasing the local membrane resistance. On the other hand, if reactants are oversaturated, too much water will be present near the outlet leading to GDL pore blocking (flooding).

Cleghorn et al. [8] studied the effect of increasing the anode RH on CDD and local HFR for a SFC with multiple channels serpentine flow fields at $T_{cell} = T_{hum,c} = 80\,^{\circ}C$, $Q_{air} = 5000\ ml\ min^{-1}$ and hydrogen flow rate ($Q_{H_2}$) of $700\ ml\ min^{-1}$. Three RH conditions were considered for the anode, $T_{hum,a} = 80$ and $T_{hum,a} = 100\,^{\circ}C$ and dry condition. The oversaturated condition showed highest, more homogeneous current density and the lowest, more homogeneous HFR. The other cases showed an increase in current density and a decrease in HFR towards the outlet, with a better performance for the saturated condition. Sun et al. [84] analyzed the effect of increasing the anode RH for: (i) dry cathode feed and (ii) saturated cathode feed. For the first case $T_{cell} = 59.85\,^{\circ}C$ and for the second $T_{cell} = 69.85\,^{\circ}C$. For the first case, $Q_{H_2} = 250\ ml\ min^{-1}$ and $Q_{air} = 700\ ml\ min^{-1}$, for the second, $Q_{H_2} = 200\ ml\ min^{-1}$ and $Q_{air} = 600\ ml\ min^{-1}$. Each run lasted 6.5 h and the $T_{hum,a}$ was gradually increased from $39.85\,^{\circ}C \leq T_{hum,a} \leq 89.85\,^{\circ}C$ starting at non-humidified conditions. For the first case (dry cathode feed), and even at oversaturated conditions of the anode, the membrane never reached a fully hydrated state and the local current density increased towards the outlet. For the second case (saturated cathode feed), the cell showed a steadily decrease in current densities from the inlet to the outlet accentuated at anode oversaturated conditions as a result of flooding.

Noponen et al. [59] studied the effect of feeding pure oxygen with two different RH. These authors considered a segmented cell with an anodic net/grid geometry flow field and a cathodic special flow field with multiple inlets and outlets. For the studies, $T_{hum,a} = T_{cell} = 60\,^{\circ}C$, $\lambda_{H_2} = 3.4$ and $\lambda_{O_2} = 5.5$. The $T_{hum,c} = 60\,^{\circ}C$ for the high humidity and $T_{hum,c} = 40\,^{\circ}C$ for the low RH conditions. The high RH condition showed a more uniform CDD. The low RH condition showed a slight increase in current density towards the cell outlet attributed to improved proton conductivity and a dryer state of the polymer near the inlet. Yoshioka et al. [37] performed CDD measurements at various fuel and oxidant stoichiometries for $T_{cell} = 75\,^{\circ}C$ and $T_{hum,a} = T_{hum,c} = 65\,^{\circ}C$. For the experiments hydrogen and air stoichiometries ranged between 1.25 and 2.5. The CDD profiles obtained are shown in Fig. 11. It is observed on the CDD profiles, that under low RH conditions the current density depends only on the stoichiometry of air. These authors concluded that the region with higher current density for $\lambda_{H_2} = 1.3$ and $\lambda_{O_2} = 2.5$, tend to move upwards the flow field gas channel for long-term (250 h) operating regimes. Similar results have been reported by other research groups [8,57,108].

Yoon et al. [54] analyzed the flooding effect on CDD. A saturated and two oversaturated conditions (~300% RH and ~600% RH) were tested for both the anode and cathode at $T_{cell} = 27\,^{\circ}C$, $\lambda_{H_2} = 1.25$ and $\lambda_{O_2} = 2.5$. They concluded that the flooding process begins at the outlet and progressively moves towards the inlet of the cell.

Reum et al. [82] used their segmented cell with sub-millimeter resolution to measure the CDD under the ribs and under gas channels of the flow field at different RH conditions. For the experiments, $T_{cell} = 70\,^{\circ}C$, $\lambda_{H_2} = 23$ and RH = 40%. The cathode was fed with air ($\lambda_{air} = 10$) and oxygen ($\lambda_{O_2} = 46$) for RH between 0 and 100%. Higher current densities and lower ohmic resistances were observed under the gas channels of the flow field at higher RH and were attributed to the fact that the gas channels area has lower mass transport restrictions compared to the flow field ribs. They also found that the local membrane resistance changes mainly under the gas channel as a result of the limited membrane humidification under the rib covered zones.

### 3.4. Reactants flow rate

CDD measurements can provide information about specific zones of the cell where reactants are insufficient (fuel or oxidant starvation). In PEMFC, the performance is extremely sensitive to cathode stoichiometry due to relatively sluggish oxygen reduction reaction (ORR) kinetics and mass transport [36]. At the same time, operating the anode under low stoichiometric conditions may originate cell reversal, resulting in water oxidation. The oxygen produced in the water oxidation reaction can then react with the hydrogen producing excessive local heat that degrades the catalyst [87]. The responsible mechanisms for depletion of the reactants along the flow field channels are: upstream consumption which is traduced in a scarcity of reactants downstream, blockage of the flow field channel, inadequate water removal from the flow field channels and restricted access of reactants to the electrode due to poorly designed flow fields [73].

Natarajan and Nguyen [45] studied the effect of hydrogen starvation in a straight single channel segmented cell with five segments (organized as a horizontal row) at $T_{cell} \approx 30\,^{\circ}C$, $T_{hum,a} = 40\,^{\circ}C$, $T_{hum,c} = 30\,^{\circ}C$, $Q_{H_2} = 5.1\ ml\ min^{-1}$ and oxygen flow rate ($Q_{O_2}$) of $19\ ml\ min^{-1}$. Current density was tracked during 30 min for 0.70, 0.60 and 0.55 V. When segments were at 0.70 V, hydrogen was in excess for the reaction and current densities were stable for all segments. For 0.6 V, starvation effects were observed in segments four and five as more than 70% of the hydrogen was consumed at the three first segments. Finally, at 0.55 V the starvation effects were observed in segments three, four and five, with the last two generating almost no current.

Büchi et al. [57] operated a segmented cell of technical relevance ($200\ cm^2$ cell active area) at different oxidant stoichiometries $1.1 \leq \lambda_{air} \leq 3$. Other operating conditions were $\lambda_{H_2} = 2$, $T_{cell} = T_{hum,a} = T_{hum,c} = 70\,^{\circ}C$. Galvanostatic tests were performed at approximately $400\ mA\ cm^{-2}$. It was observed that at low stoichiometries, $1.1 \leq \lambda_{air} \leq 1.5$, the first two segments were

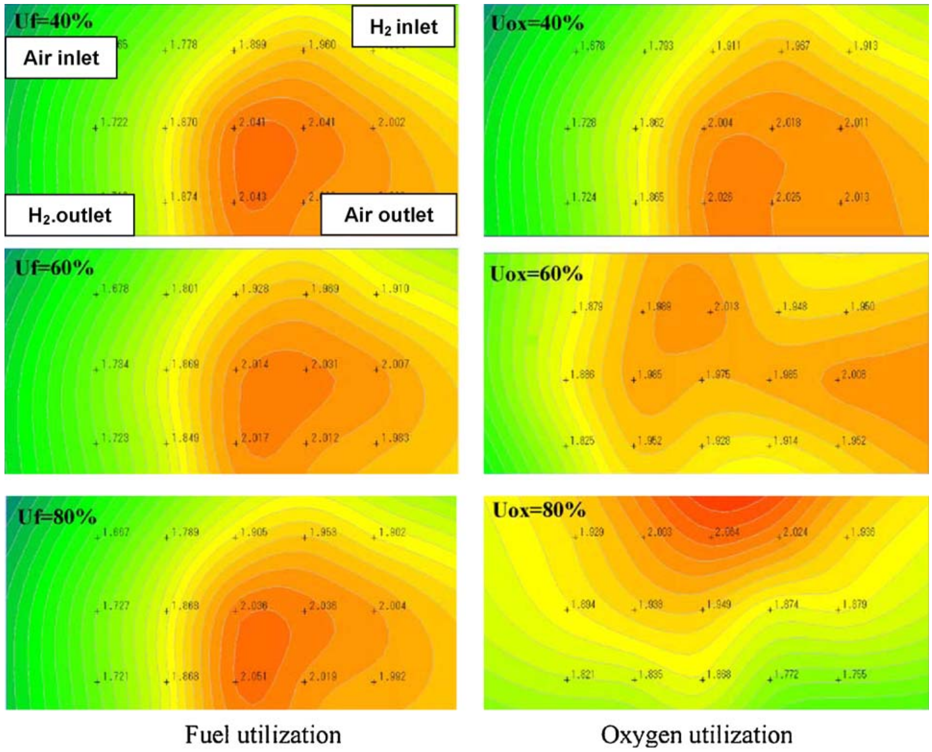



**Fig. 11.** Current distributions at different gas utilizations. Left figures—the influence of fuel utilization at a constant oxygen utilization of 40%. Right figures—the influence of oxygen utilization at a constant fuel utilization of 75%. Average current density is set at 0.25 A cm$^{-2}$. The temperatures are kept at a constant of 75 °C by circulation of coolant. Dew points of gases are kept at a constant of 65 °C.Adapted from Ref. [37] with permission.

producing most of the current due to oxidant depletion along the flow field path. At higher stoichiometries, $\lambda_{air} > 1.5$, the CDD became relatively homogeneous. These results are shown in Fig. 12 where segment one is located at the inlet and segment four at the outlet of the cell. Other authors have observed relatively homogeneous CDD at $\lambda_{air} \geq 2.9$ [8] and $\lambda_{air} \geq 2$ [28]. Both the fuel [40,80] and oxidant [53,68,73] starvation condition have further been studied leading to similar results.

Concerning DMFC, to study the effect of low oxidant stoichiometry on the CDD has served to confirm the bifunctional operating regime (BFR) of this type of cell proposed by Ye et al. [89] and Ye and Zhao [90]. In this way, it has been found by several authors that the number of current generating (galvanic) zones tends to increase along with the oxidant stoichiometry, reducing the current consuming, hydrogen generating (electrolytic) zones [11,18]. Dohle et al. [22] investigated the BFR of DMFC for $T_{cell}$ = 70 °C and a methanol mass flow rate of 17 kg h$^{-1}$ with 1 M concentration. Different air flow rates were used ranging between 0 ml min$^{-1}$ $\leq Q_{air} \leq$ 2000 ml min$^{-1}$. The CDD was measured at OCV conditions and the location of the hydrogen generating zones was highlighted. More electrolytic zones and higher internal currents were observed at lower $Q_{air}$. Fig. 13 shows the CDD profile for $Q_{air}$ = 400 ml min$^{-1}$, which represents the case with maximum internal currents (12 A) reported by these authors.

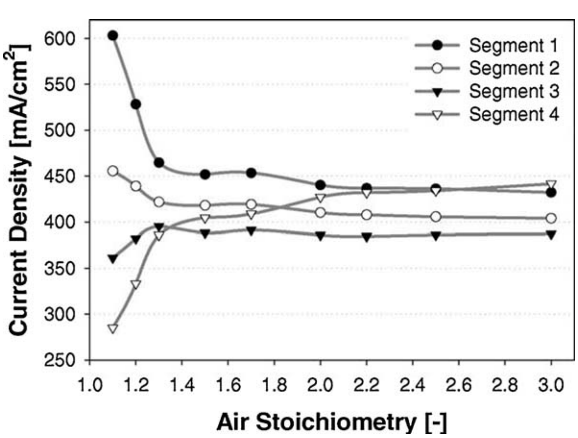



**Fig. 12.** Deviation of current density from average current density in the segments 1–4 as function of total cell current. Cell operated in constant flow mode with gas flows rates corresponding to $\lambda_{H_2} = 2$ and $\lambda_{air}$ = 1.5@80 A total cell current (400 mA cm$^{-2}$). $T_{cell} = T_{hum,a} = T_{hum,c}$ = 70 °C.From Ref. [57] with permission.

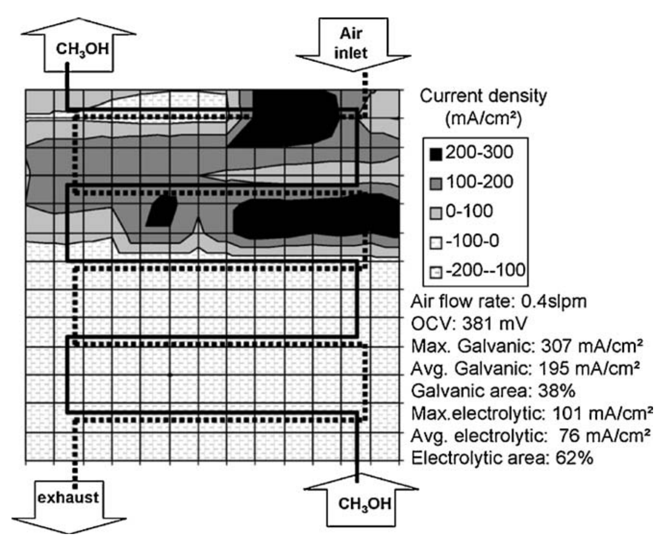



**Fig. 13.** Local current densities with air supply of 0.4 l min$^{-1}$ at OCV; anode mass flow rate 17 kg h$^{-1}$; methanol concentration 1 M.From Ref. [22] with permission.

### 3.5. Operating pressure

According to the Nernst equation, improvements in PEMFC performance can be achieved at higher operating pressures [83]. However, in real fuel cell systems exist a trade-off as operating a PEMFC at low (≈ambient) pressures reduces the parasitic power losses due to fans or compressors. The effect of operating pressure on CDD was studied by Liu et al. [33] at different air ($P_{air}$) and $H_2$ ($P_{H_2}$) inlet pressures of the reactants. The operating parameters were $T_{cell} = T_{hum,a} = T_{hum,c} = 75\,^{\circ}C$, $\lambda_{H_2} = \lambda_{O_2} = 2$; $P_{air} = P_{H_2} = 2$ bar for the first run and for the second. As expected, the overall performance was slightly lower at $P_{air} = P_{H_2} = 2$ bar. For the lower operating pressure, the CDD profile was progressively more uneven at higher current densities, decreasing from inlet to outlet. The last was attributed to: (i) flooding, as more water (∼50%) was brought into the cell and (ii) reduced oxygen partial pressure along the flow field channel. Similar studies were performed by Ghosh et al. [34] and Sun et al. [68]. In both cases, increasing the pressure of reactants led to a performance increase in the segments closer to the inlet and to a performance decrease towards the outlet. These authors demonstrated that operating a SFC at higher pressures may not be advantageous as it can lead to a poorer performance of the downstream zones of the flow field.

### 3.6. Contaminant species

If PEMFC systems are operated on hydrogen obtained from reformed hydrocarbons (e.g. methane) or alcohols (e.g. methanol), small amounts of CO will be present. In the same way it is accepted that the concentration of CO must not exceed 10 ppm for low temperature operation (<90 °C), otherwise the PEMFC performance will suffer important losses due to poisoning of the Pt electrocatalyst [83]. For some researchers, it has been of interest to study the effect of incorporating small amounts (<100 ppm) of CO, $CO_2$ and $NO_2$ on the hydrogen feed and analyze its effect on the CDD. The addition of these species aims to understand how the deactivation processes of Pt-based catalysts are spatially distributed over the MEA active area as they can be directly related to a decrease in local current density [92]. Tingelöf et al. [94] performed CDD measurements in a segmented cell operated on a reformate mix composed by 50% $H_2$, 40% $CO_2$ and 10% $N_2$ at two different CO concentration levels, 10 and 80 ppm. These authors also evaluated the efficiency of air bleeding for CO poisoning mitigation and the CO and $CO_2$ tolerance on Pt/C and PtRu/C catalysts. During the tests, reactants were fed with 100% RH, $\lambda_{H_2} = 1.5, \lambda_{O_2} = 2.4$, $T_{cell} = 60\,^{\circ}C$ and ambient pressure. Independently of the catalyst, it took ∼60 min for the CDD to reach a steady state when 10 ppm of CO were added to the reformate mix. It was also observed that $CO_2$ did not affect significantly the CDD. To recover from lower CDD profiles, an air bleed level of approximately 0.5% for each 10 ppm of CO was needed during potentiostatic tests at 680 mV—Fig. 14. Concerning the catalysts, it was found that the CO adsorbed more strongly onto the Pt/C than onto the PtRu/C catalyst. The last effect was strengthened when the cell was operated in potentiostatic mode due to the impossibility of the anodic polarization to reach the required potential for CO oxidation. A similar study was presented by Stumper et al. [58] who, operating a segmented cell under very similar conditions, needed approximately 1% of oxygen to recover the previous voltage of the cell after introducing a reformate containing 40 ppm of CO.

St-Pierre et al. [112] studied the effect of $NO_2$ on the CDD. For operating conditions: $\lambda_{H_2} = 1.6, \lambda_{O_2} = 2$, $65\,^{\circ}C \leq T_{cell} \leq 75\,^{\circ}C$ and $T_{hum,a} = T_{hum,c} = 72\,^{\circ}C$, the hydrogen gaseous stream was poisoned with 0.01, 0.1 and 0.75 ppm of $NO_2$. It was noted that the CDD varied less than 5% after 55.8 h of operation. The voltage

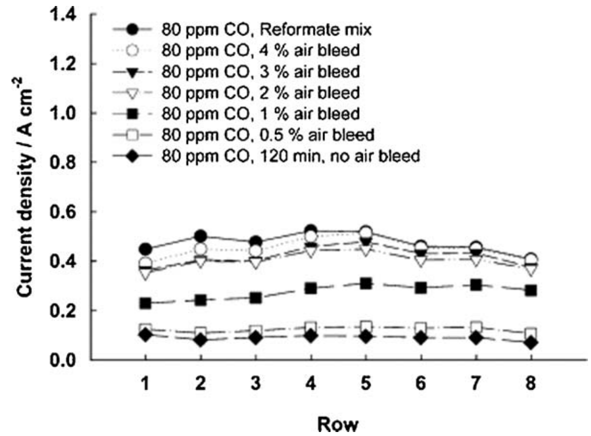



**Fig. 14.** Potentiostatic (680 mV) current distribution steady-state of PtRu/C for different levels of air in 80 ppm CO, 50% $H_2$, 40% $CO_2$ and 10% $N_2$ (reformate mix). Stoichiometry cathode 2.4, anode 1.5. Cell temperature 60 °C. RH 100%. Pressure ambient.From Ref. [94] with permission.

was monitored during the same period time and showed an average decrease of ∼40 mV. These authors observed two different trends for the $NO_2$ contamination process, a linear decay in early stages (with an increased slope at higher $NO_2$ concentration levels) followed by a steady-state value reached for a long operating time.

### 3.7. Membranes and GDL

In this section is discussed the effect of using membranes or GDL of different types and characteristics on the CDD profile. There are, though, very few studies reporting on this subject. Weng et al. [49] studied the transient evolution of the CDD using Nafion® 112 (thickness = 50.8 μm) and Nafion® 117 (thickness = 175 μm) membranes operated under low RH conditions. The tests involved the use of E-Tek 250-W electrodes. $H_2$ and air were supplied at three RH conditions, 100%, 50% and dry, $\lambda_{H_2} = 1.2$, $\lambda_{air} = 2$ and $T_{cell} = 50\,^{\circ}C$. These authors concluded that the Nafion® 112 membrane is more suitable for low RH conditions due to better proton conductivity and more uniform performance at any position of the multiple channels serpentine flow fields. When operated under low RH conditions, Nafion® 117 membrane showed uneven performances along the flow field. Recently, Pérez et al. [55] performed CDD measurements using two different membranes, namely a Nafion® 112 and Fumapen® F-950 both with ∼50 μm thick and similar proton conductivities ∼0.1 S cm$^{-1}$. Similar CDD profiles were obtained for both membranes with current densities between 240 and 390 mA per segment (∼1.56 cm$^2$ area) for the Nafion® 112 and between 170 and 375 mA per segment for the Fumapen® F-940. The cell was operated at $T_{cell} = 30\,^{\circ}C$, $Q_{H_2} = 200$ ml min$^{-1}$, $Q_{air} = 1500$ ml min$^{-1}$, dry hydrogen and 95% RH of air. The low current density at the inlet (segment 1, 1) was associated to the drying effect of hydrogen. The low current density towards the outlet was attributed to the lack of hydrogen (starvation effect) as most of the hydrogen was being consumed in the middle segments of the cell. The CDD profiles for both membranes are shown in Fig. 15.

Hicks et al. [10] investigated the effect of three different GDL on the CDD. The GDL selected were made of flexible non-woven, rigid non-woven paper and flexible woven materials, all of them were not segmented. Two air flow rates, 200 and 500 ml min$^{-1}$, were applied. Other parameters were: $Q_{H_2} = 200$ ml min$^{-1}$, RH = 90% for both gases and $T_{cell} = 75\,^{\circ}C$. Multiple channels serpentine flow fields were used. The GDL made of rigid non-woven paper showed the most uniform CDD. The rigid non-woven paper and the flexible

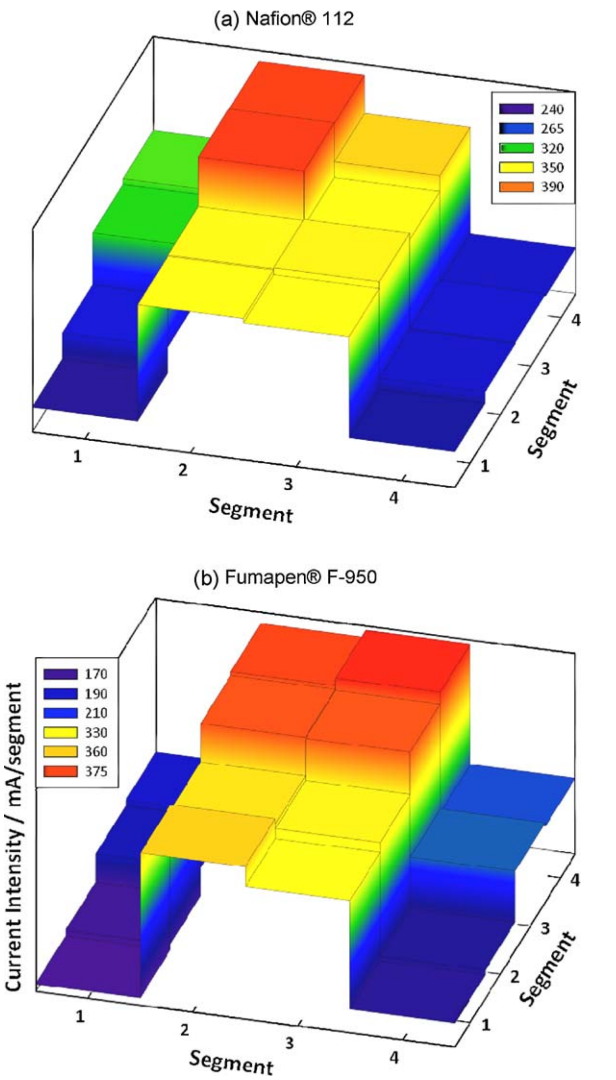



**Fig. 15.** Current density distribution profiles for two different MEAs. GDL: ElectroChem® 0.5 mg cm$^{-2}$ (10 wt.% Pt/C). Current density distribution taken at $V_{cell}$ = 638 mV. Counter flow feeding with $H_2$ inlet at coordinate (1, 1) and outlet at (4, 4). Anode: $H_2$, $Q$ = 200 ml min$^{-1}$, $P$ = 1.25 bar, dry. Cathode: Air, $Q$ = 1500 ml min$^{-1}$, $P$ = 1 bar, RH = 95%. $T_{cell}$ = 30 °C.

woven showed very similar and more uniform CDD for the higher air flow rate case. These authors concluded that the impact of GDL on the CDD profile of a SFC is less important than the effect of air flow rate.

Regarding DMFC, Saarinen et al. [91] performed CDD measurements in order to compare two membranes with similar conductivity and different permeation rates to methanol namely, a poly(vinylidene fluoride)-graft-poly(styrene sulfonic acid) (PVDF-g-PSSA) and a Nafion® 117 membrane. The conductivity was 4.5 and 5 S m$^{-1}$, respectively, while the methanol permeation rate was higher (not specified) for the former. The DMFC was free-breathing type and the MEA was assembled with commercial electrodes in both cases. For the experiments, 30 °C ≤ $T_{cell}$ ≤ 70 °C, 0.198 ml min$^{-1}$ ≤ $Q_{met}$ ≤ 7.8 ml min$^{-1}$ and methanol concentration ranged between 0.5 and 10 M. For methanol concentrations above 3 M more uneven CDD profiles were observed; that was attributed to higher methanol crossover rates. The maximum power densities were observed for the 1 M methanol concentration on both membranes, with no remarkable changes at higher flow rates. However, lower power densities (20–50% less) were observed for the PVDF-g-PSSA membrane.

**Table 3**
References using complementary analytical techniques in SFC for distributed analysis.

| Experimental technique | References |
|---|---|
| Gas composition analysis ($H_2$, $O_2$, $H_2O$) | [21,32,50,78,79,101,102] |
| Water accumulation | |
| Direct liquid water visualization techniques | [19,31,44,80] |
| Neutron radiography | [25,74,107,115] |
| Temperature distribution | [10,11,16,44,53,64,69,80] |
| HFR | [8,25,28,32,48,53,59,78–81] |
| EIS | [46,49,61,73–77] |

## 4. Integrated analytical techniques

As mentioned before, the simplest way to study the distributed electrochemical performance over the MEA active area is to measure the CDD. Nonetheless, complementary analytical techniques that permit the distributed measurement of gas composition analysis, water accumulation, temperature, HFR and EIS have been successfully integrated in SFC, allowing researchers to obtain further understanding of PEMFC systems. The importance of combining CDD measurements with the analytical techniques presented in this section relies on the fact that the performance of PEMFC is hardly influenced by the complex interaction of the parameters previously mentioned. Table 3 summarizes the analytical techniques that have been combined with CDD measurements.

It is important to highlight that, the integration of distributed HFR and EIS was first reported by Cleghorn et al. [8] and Brett et al. [61] using the PCB technique. As it is beyond the scope of this work only the combination of local EIS with a water accumulation technique is presented below.

### *4.1. Gaseous species distribution*

The measurement of local gaseous species along the flow field channels of SFC provides important information about the concentration of reactant species and water vapor inside the cell (e.g. to track the oxygen depletion and water formation along the channels). Mench and Wang from the Pennsylvania State University used gas chromatography to measure the steady-state [102] and real-time [78,79] distribution of $H_2$, $O_2$, $N_2$ and water vapor in segmented cell. To do that, 16 extraction ports (8 per electrode) equally spaced along the serpentine flow field of single channel were created. The extraction ports were connected to a GC for analysis during steady state operation. In a similar form, the extraction ports were connected to a real-time gas analyzer for transient analyses. The sampling flow rate needed for this analyzer was less than 3% of the flowing stream in the channel. In a following report [50], these authors calculated local values of the net water transport coefficient across the membrane ($\alpha$). The coefficient was calculated from CDD measurement and local molar fraction of water in the anode. Fig. 16 depicts the different values obtained for $\alpha$; positive values mean a net transport of water from the anode to the cathode. In other words, positive values of $\alpha$ mean that the electro-osmotic drag (EOD) of water is the dominant water transport mechanism across the membrane while negative values mean that the water back diffusion dominates over the EOD.

Nishikawa et al. [21] performed local RH and CDD measurements in cell with three segments. RH was measured by drilling six 1 mm diameter holes in the cathodic flow field. To each of these six holes it was then connected a RH meter. The operating conditions were: $T_{cell}$ = $T_{hum,a}$ = 80 °C and 40 °C ≤ $T_{hum,c}$ ≤ 70 °C. For $T_{hum,c}$ = 40 °C the RH of air at the inlet was 30%. However, from the RH measurements it was observed a gradual increase up to 70% towards the outlet, highlighting the large difference that can appear even at relatively small current densities (≈0.150 mA cm$^{-2}$). The CDD measurements

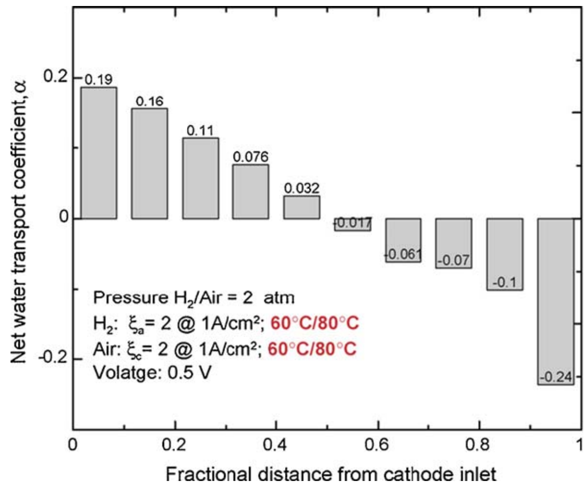



**Fig. 16.** Net water transport coefficient profile for the humidifier temperature of 60 °C in both anode and cathode. The cell temperature is 80 °C.From Ref. [50] with permission.

started at $T_{hum,c}$ = 70 °C which gradually decreased to $T_{hum,c}$ = 40 °C. The results were in accordance with the local RH measurements showing an increasingly better performance for the downstream segment when $T_{hum,c}$ = 40 °C and the local RH difference between the inlet and the outlet was larger.

### 4.2. Condensed water accumulation

To correlate the liquid water distribution with the local electrochemical performance segmented cells, it is important to use tools that allow researchers to have an idea about the actual liquid water accumulation state at the gas channels, mainly at the cathode. The easiest way to monitor the water accumulation is by disassembling the SFC after a certain period of operation [19]; however, this technique is time consuming and not quantitative. The direct observation of condensed water accumulation at the gas channels of operating SFC can be achieved by using transparent materials for pertinent PEMFC components. Then, a coupled charge device (CCD) camera [44,80] or a digital camera [31,53] can be used to observe the water accumulation inside the flow fields.

A more sophisticated technique to visualize the distribution of water is neutron radiography (NR). A review of the use of NR for water visualization in PEMFC was recently presented by Mukundan and Borup [106]. When implemented in SFC, the materials used in the cell must have improved neutron transparency [25]. Schneider et al. [74] performed simultaneous local EIS and NR in a 29.2 cm$^2$ active area PEMFC operating on pure $H_2$ and $O_2$. Three technical modifications were made to ensure high neutron transparency: (i) the endplates were fabricated of 3 cm thick gold plated aluminum blocks, (ii) the cathode current collector was built in anodized aluminum plate and (iii) graphite flow fields thickness was reduced to 2 mm for the anode and 3 mm for the segmented cathode to minimize attenuation of the neutron beam by this material. Fig. 17 depicts the main results obtained. It was observed that under low humidity conditions, simultaneous severe drying zones at the inlet and flooded zones at the outlet can appear when operating a PEMFC in co-flow mode. This has also been reported by other authors in counter flow mode [37]. The combination of NR and CDD measurements showed a partially flooded transition zone between undersaturated and completely flooded parts of the cell. From the local EIS measurements it was concluded that near the inlet, poor interfacial kinetics due to drying of the ionomer at the catalyst layer of the electrodes might exceed the impact of increased membrane resistance.

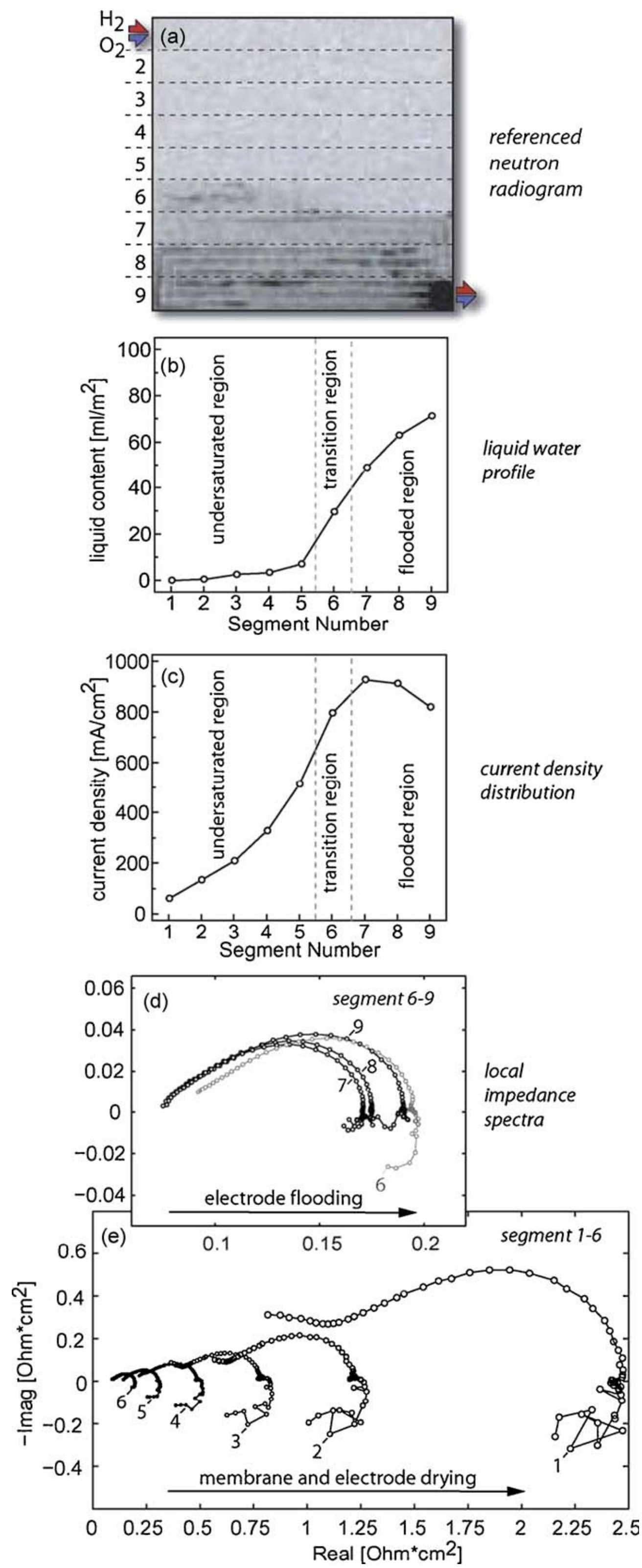



**Fig. 17.** Results in co-flow mode: $T_{cell}$ = 70 °C, $I_{cell}$ = 14.6 A, $A_{cell}$ = 29.2 cm$^2$, $\lambda_{H_2} = \lambda_{O_2} = 1:5$, RH ($H_2$) = 40%, dry $O_2$, $f_{mod}$ = 10 mHz to 10 kHz, Nafion® 112 membrane, ETEK ELAT V3.1 electrodes, 250 μm PTFE gaskets (numbers denote segment).From Ref. [74] with permission.

Recently, Schröder et al. [107] performed for the first time NR and CDD measurements DMFC. These authors concluded that it is possible to correlate the production of water and $CO_2$ at the cathode of DMFC using NR and CDD distribution measurements.

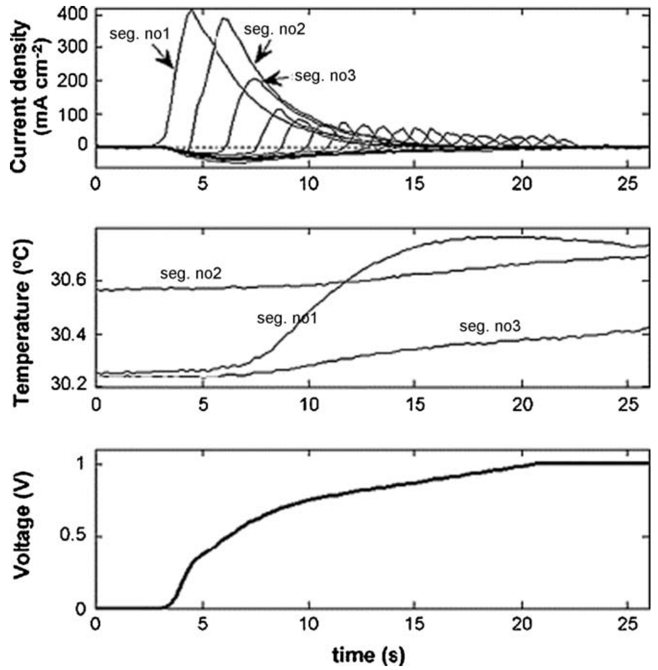



**Fig. 18.** Voltage rise and evolutions of local temperatures and current densities when hydrogen is introduced in an anode full of air (fuel cell at open circuit).From Ref. [53] with permission.

### 4.3. Temperature distribution

By mapping the temperature distribution along the MEA active area, it is possible to locate the zones with higher electrochemical activity as the local heat generation increases with current density according to Joule's laws [105]. Hakenjos et al. [44] performed temperature distribution measurements by placing a zinc selenide window (transparent to infrared and visible light) immediately after the cathodic flow field. The temperature distribution measurements were performed with an infrared camera. The operating conditions were 250 ml min$^{-1}$ $\leq Q_{air} \leq$ 750 ml min$^{-1}$, $T_{cell} = T_{hum,c}$ = 23 °C and $Q_{H_2} = 100$ ml min$^{-1}$, dry. At the highest air flow rate, no liquid water was observed, in this case it was verified a direct correspondence between local temperature and local current densities. On the contrary, these authors observed areas with higher temperature and lower current density in flooded zones of the cell at lower air flow rates (250 and 500 ml min$^{-1}$). In these cases, the condensed water led to lower current densities by hindering the gas transport through the porous media of the GDL and covering the catalytic active surface. The higher temperatures in flooded zones were attributed to the water condensation enthalpy.

Maranzana et al. [53], measured the local temperature using 20 thermocouples (one per segment) inserted into a rib channel at different positions of the cathode flow field. They observed a rise in temperature near the inlet when hydrogen was fed to the cell at OCV condition. The rise was attributed to internal currents of nominal value up to 0.4 A cm$^{-2}$ generated by the simultaneous oxidation of hydrogen and residual oxygen (present in the flow field before hydrogen being fed to the cell) at the anode—Fig. 18.

## 5. Conclusions

The performance of PEMFC is uneven over the MEA active area and depends on a complex interaction of various design, assembling and operating parameters as well as on the properties and microstructure of the materials used. To the date, SFC have proven to be an excellent diagnostic tool that permits further understanding of the local electrochemical performance in single cells and stacks.

SFC can be classified accordingly to common structural concepts in: printed circuit board, resistors network and Hall effect sensors. The Hall effect sensors technique can be considered as the most accurate for local electrochemical characterization, due to the possibility of calibration of these current sensing devices, followed by the resistors network and the PCB. The accuracy of the electrochemical measurements can be improved significantly by segmenting the GDL, the BP and the CC. The PCB technique is the most suitable for use in middle cells of PEMFC stacks as it offers the possibility of incorporating the segmented flow fields of adjacent cells.

CDD measurements have been crucial to understand the effect of flow field geometry, clamping pressure, reactants relative humidity and flow rate, operating pressure, contaminant species, membrane thickness and GDL on the performance of PEMFC. Despite its importance concerning fuel cells durability, there is a lack of literature describing suitable strategies to homogenize the CDD in PEMFC systems.

Regarding DMFC, CDD measurements have been especially important to confirm the simultaneous existence of electrolytic and galvanic operating regions showed by this type of cell at low oxidant stoichiometric rates.

The integration of various analytical techniques that allow: (i) $H_2$, $O_2$, $N_2$ and $H_2O$ distribution determination, (ii) condensed water distribution evaluation, (iii) temperature distribution and (iv) local high frequency resistance (HFR) and local electrochemical impedance spectroscopy (EIS) analysis have been reported. These techniques provide important information that complements the CDD measurements.

PEMFC *in situ* diagnostic methods need to be improved and standardized as they should play a key role in the massive commercialization of PEMFC systems. In this way, SFC can be used to optimize PEMFC systems as they provide fast and reliable *in situ* measurements that allow to evaluate how the interaction of different parameters affect the local and overall performance. Present applications of SFC include the diagnosis of PEMFC components manufacturing defects of [120] and the study of PEMFC distributed startup at sub-zero temperatures [121]. SFC have never been reported for high-temperature PEMFC (operating above 100 °C) despite this recent type of cells are receiving increasingly attention.

## Acknowledgments

Luis C. Pérez is grateful to FCT for his PhD grant reference SFRH/BD/44684/2008. Lúcia Brandão is also thankful to FCT for her post-doc grant (SFRH/BPD/41233/2007). Financial support by FCT through the project PTDC/EQU-EQU/70574/2006 is also acknowledged.

## References

[1] Carrette L, Friedrich KA, Stimming U. Chemphyschem 2000;1:162–93.
[2] Holladay JD, Hu J, King DL, Wang Y. Catal Today 2009;139:244–60.
[3] David E. J Mater Process Technol 2005;162–163:169–77.
[4] Agnolucci P. Int J Hydrogen Energy 2007;32:3526–44.
[5] Wee J-H. Renew Sustain Energy Rev 2007;11:1720–38.
[6] Kandlikar SG, Lu Z. J Fuel Cell Sci Technol 2009;6:044001.
[7] Bruijn F. In: Handoko LT, Masbah RTS, editors. PEM fuel cells for transport applications: state of the art and challenges. AIP; 2009. p. 3–12.
[8] Cleghorn SJC, Derouin CR, Wilson MS, Gottesfeld S. J Appl Electrochem 1998;28:663–72.
[9] Rajalakshmi N, Raja M, Dhathathreyan KS. J Power Sources 2002;112:331–6.
[10] Hicks M, Kropp K, Schmoeckel A, Atanasoski R. ECS Trans 2006;1:605–12.
[11] Sauer DU, Sanders T, Fricke B, Baumhöfer T, Wippermann K, Kulikovsky AA, et al. J Power Sources 2008;176:477–83.
[12] Bender G, Wilson MS, Zawodzinski TA. J Power Sources 2003;123:163–71.
[13] Yuan XZ, Wang HJ, Sun JC, Zhang JJ. Int J Hydrogen Energy 2007;32:4365–80.
[14] Wu JF, Yuan XZ, Wang HJ, Blanco M, Martin JJ, Zhang JJ. Int J Hydrogen Energy 2008;33:1747–57.
[15] Wang C-Y. Chem Rev 2004;104:4727–66.

[16] Abdullah AM, Okajima T, Mohammad AM, Kitamura F, Ohsaka T. J Power Sources 2007;172:209–14.
[17] Freunberger SA, Reum M, Wokaun A, Büchi FN. Electrochem Commun 2006;8:1435–8.
[18] Kulikovsky AA, SchrnitZ H, Wippermann K, Mergel J, Fricke B, Sanders T, et al. Electrochem Commun 2006;8:754–60.
[19] Hsieh SS, Huang YJ. J Power Sources 2008;183:193–204.
[20] Wieser C, Helmbold A, Gulzow E. J Appl Electrochem 2000;30:803–7.
[21] Nishikawa H, Kurihara R, Sukemori S, Sugawara T, Kobayasi H, Abe S, et al. J Power Sources 2006;155:213–8.
[22] Dohle H, Mergel J, Ghosh PC. Electrochim Acta 2007;52:6060–7.
[23] LaDou J. Int J Hyg Environ Health 2006;209:211–9.
[24] Schulze M, Gulzow E, Schonbauer S, Knori T, Reissner R. J Power Sources 2007;173:19–27.
[25] Gagliardo JJ, Owejan JP, Trabold TA, Tighe TW. Nucl Instrum Methods Phys Res Sect A Accel Spectrom Detect Assoc Equip 2009;605:115–8.
[26] Brett DJL, Atkins S, Brandon NP, Vesovic V, Vasileiadis N, Kucernak AR. Electrochem Commun 2001;3:628–32.
[27] Strickland DG, Litster S, Santiago JG. J Power Sources 2007;174:272–81.
[28] Morimoto Y, Suzuki T, Yamada H. Electrochem Soc Proc 2002;31:248–56.
[29] Noponen M, Mennola T, Mikkola M, Hottinen T, Lund P. J Power Sources 2002;106:304–12.
[30] Benziger J, Chia JE, Kimball E, Kevrekidis IG. J Electrochem Soc 2007;154: B835–44.
[31] Tabe Y, Kikuta K, Chikahisa T, Kozakai M. J Power Sources 2009;193:416–24.
[32] Araki T, Koori H, Taniuchi T, Onda K. J Power Sources 2005;152:60–6.
[33] Liu Z, Mao Z, Wu B, Wang L, Schmidt VM. J Power Sources 2005;141:205–10.
[34] Ghosh PC, Wuster T, Dohle H, Kimiaie N, Mergel J, Stolten D. J Power Sources 2006;154:184–91.
[35] Ay F, Ata A, Dohle H, Sener T, Gorgun H. J Power Sources 2007;167:391–7.
[36] Mench MM, Wang CY, Ishikawa M. J Electrochem Soc 2003;150:A1052–9.
[37] Yoshioka S, Yoshimura A, Fukumoto H, Hiroi O, Yoshiyasu H. J Power Sources 2005;144:146–51.
[38] Bansal R. Fundamentals of engineering electromagnetics. Florida: Taylor & Francis Group; 2006.
[39] http://content.honeywell.com/sensing/prodinfo/solidstate/technical/chapter2.pdf, retrieved on February 2010.
[40] Liang D, Shen Q, Hou M, Shao Z, Yi B. J Power Sources 2009;194:847–53.
[41] Santis M, Freunberger SA, Papra M, Wokaun A, Büchi FN. J Power Sources 2006;161:1076–83.
[42] Rieke PC, Vanderborgh NE. J Electrochem Soc 1987;134:1099–104.
[43] Vermeijlen JJTT, Janssen LJJ, Geurts AJ, Haastrecht GC. J Appl Electrochem 1995;25:1122–7.
[44] Hakenjos A, Muenter H, Wittstadt U, Hebling C. J Power Sources 2004;131: 213–6.
[45] Natarajan D, Van Nguyen T. AIChE J 2005;51:2587–98.
[46] Schneider IA, Kuhn H, Wokaun A, Scherer GG. J Electrochem Soc 2005;152:A2092–103.
[47] Geiger AB, Eckl R, Wokaun A, Scherer GG. J Electrochem Soc 2004;151:A394–8.
[48] Hakenjos A, Tüber K, Schumacher JO, Hebling C. Fuel Cells 2004;4:185–9.
[49] Weng FB, Jou BS, Li CW, Su A, Chan SH. J Power Sources 2008;181:251–8.
[50] Lu GQ, Liu FQ, Wang CY. J Power Sources 2007;164:134–40.
[51] Natarajan D, Van Nguyen T. J Power Sources 2004;135:95–109.
[52] Hwnag JJ, Chang WR, Peng RG, Chen PY, Su A. Int J Hydrogen Energy 2008;33:5718–27.
[53] Maranzana G, Lottin O, Colinart T, Chupin S, Didierjean S. J Power Sources 2008;180:748–54.
[54] Yoon YG, Lee WY, Yang TH, Park GG, Kim CS. J Power Sources 2003;118:193–9.
[55] Martínez LC, Brandão L, Sousa JM, Mendes A. PEMFC study using a segmented fuel cell. In: HYCELTEC 2009–II Iberian Symposium on Hydrogen, Fuel Cells and Advanced Batteries; 2009 [ref. P19-SA].
[56] Eckl R, Grinzinger R, Lehnert W. J Power Sources 2006;154:171–9.
[57] Büchi FN, Geiger AB, Neto RP. J Power Sources 2005;145:62–7.
[58] Stumper J, Campbell SA, Wilkinson DP, Johnson MC, Davis M. Electrochim Acta 1998;43:3773–83.
[59] Noponen M, Ihonen J, Lundblad A, Lindbergh G. J Appl Electrochem 2004;34:255–62.
[60] Siroma Z, Fujiwara N, Loroi T, Yamazaki S, Senoh H, Yasuda K, et al. J Power Sources 2007;172:155–62.
[61] Brett DJL, Atkins S, Brandon NP, Vesovic V, Vasileiadis N, Kucernak A. Electrochem Solid State Lett 2003;6:A63–6.
[62] Santis MV. Investigations of current density inhomogeneities in polymer electrolyte fuel cells. PhD thesis, Swiss Federal Institute of Technology Zurich; 2006.
[63] Candusso D, Poirot-Crouvezier JP, Bador B, Rullière E, Soulier R, Voyant JY. Eur Phys J Appl Phys 2004;25:67–74.
[64] Sailler S, Rosini S, Chaib MA, Voyant JY, Bultel Y, Druart F, et al. J Appl Electrochem 2007;37:161–71.
[65] Felix NB, Mathias R. Meas Sci Technol 2008;19:085702.
[66] Freunberger SA, Reum M, Evertz J, Wokaun A, Buchi FN. J Electrochem Soc 2006;153:A2158–65.
[67] Wang L, Liu H. J Power Sources 2008;180:365–72.
[68] Sun H, Zhang G, Guo L-J, Liu H. J Power Sources 2006;158:326–32.
[69] Wilkinson M, Blanco M, Gu E, Martin JJ, Wilkinson DP, Zhang JJ, et al. Electrochem Solid State Lett 2006;9:A507–11.
[70] Claycomb JR, Brazdeikis A, Le M, Yarbrough RA, Gogoshin G, Miller JH. Appl Superconduct IEEE Trans 2003;13:211–4.
[71] Yang H, Chen J, Wang S, Chen C, Jeng J, Chen J, et al. Tamkang J Sci Eng 2003;6:9–18.
[72] Hauer KH, Potthast R, Wuster T, Stolten D. J Power Sources 2005;143:67–74.
[73] Brett DJL, Atkins S, Brandon NP, Vasileiadis N, Vesovic V, Kucernak AR. J Power Sources 2007;172:2–13.
[74] Schneider IA, Kramer D, Wokaun A, Scherer GG. Electrochem Commun 2005;7:1393–7.
[75] Schneider IA, Freunberger SA, Kramer D, Wokaun A, Scherer GG. J Electrochem Soc 2007;154:B383–8.
[76] Schneider IA, Kramer D, Wokaun A, Scherer GG. J Electrochem Soc 2007;154:B770–82.
[77] Freunberger SA, Schneider IA, Sui P-C, Wokaun A, Djilali N, Buchi FN. J Electrochem Soc 2008;155:B704–14.
[78] Dong Q, Kull J, Mench MM. J Power Sources 2005;139:106–14.
[79] Dong Q, Mench MM, Cleghorn S, Beuscher U. J Electrochem Soc 2005;152:A2114–22.
[80] Hogarth WHJ, Steiner J, Benziger JB, Hakenjos A. J Power Sources 2007;164: 464–71.
[81] Holmstrom N, Ihonen J, Lundblad A, Lindbergh G. Fuel Cells 2007;7:306–13.
[82] Reum M, Freunberger SA, Wokaun A, Buchi FN. J Electrochem Soc 2009;156:B301–10.
[83] Larmaine J, Dicks A. Fuel cell systems explained, 2nd ed., 2003, West Sussex.
[84] Sun H, Zhang G, Guo L-J, Dehua S, Liu H. J Power Sources 2007;168:400–7.
[85] Sun H, Zhang G, Guo L, Liu H. Int J Hydrogen Energy 2009;34:5529–36.
[86] Ghosh PC, Wuster T, Dohle H, Kimiaie N, Mergel J, Stolten D. J Fuel Cell Sci Technol 2006;3:351–7.
[87] Taniguchi A, Akita T, Yasuda K, Miyazaki Y. J Power Sources 2004;130:42–9.
[88] Liu ZX, Yang LZ, Mao ZQ, Zhuge WL, Zhang YJ, Wang LS. J Power Sources 2006;157:166–76.
[89] Ye Q, Zhao TS, Yang H, Prabhuram J. Electrochem Solid-State Lett 2005;8:A52–4.
[90] Ye Q, Zhao TS. J Electrochem Soc 2005;152:A2238–45.
[91] Saarinen V, Himanen O, Kallio T, Sundholm G, Kontturi K. J Power Sources 2007;163:768–76.
[92] Bender G, Zawodsinski T. Electrochem Soc Proc 2002;31:212–8.
[93] Brett DJL, Atkins S, Brandon NP, Vesovic V, Vasileiadis N, Kucernak AR. J Power Sources 2004;133:205–13.
[94] Tingelöf T, Hedström L, Holmström N, Alvfors P, Lindbergh G. Int J Hydrogen Energy 2008;33:2064–72.
[95] Zhang G, Ma B, Shang D, Guo L, Sun H, Liu H. ECS Trans 2007;11:1545–52.
[96] Gülzow E, Kaz T, Reissner R, Sander H, Schilling L, Bradke Mv. J Power Sources 2002;105:261–6.
[97] Zhang GS, Guo LJ, Ma B, Liu HT. J Power Sources 2009;188:213–9.
[98] Mennola T, Noponen M, Kallio T, Mikkola M, Hottinen T. J Appl Electrochem 2004;34:31–6.
[99] Nitta I, Hottinen T, Himanen O, Mikkola M. J Power Sources 2007;171:26–36.
[100] Mench MM, Wang CY. J Electrochem Soc 2003;150:A79–85.
[101] Mench MM, Dong QL, Wang CY. J Power Sources 2003;124:90–8.
[102] Yang XG, Burke N, Wang CY, Tajiri K, Shinohara K. J Electrochem Soc 2005;152:A759–66.
[103] Stumper E, Lohr M, Hamada S. J Power Sources 2005;143:150–7.
[104] Sompalli B, Litteer BA, Gu W, Gasteiger HA. J Electrochem Soc 2007;154:B1349–57.
[105] Wang MH, Guo H, Ma CF. J Power Sources 2006;157:181–7.
[106] Mukundan R, Borup RL. Fuel Cells 2009;9:499–505.
[107] Schröder A, Wippermann K, Mergel J, Lehnert W, Stolten D, Sanders T, et al. Electrochem Commun 2009;11:1606–9.
[108] Natarajan D, Van Nguyen T. AIChE J 2005;51:2599–608.
[109] Berg P, Promislow K, Stumper J, Wetton B. J Fuel Cell Sci Technol 2005;2: 111–20.
[110] Reum M, Wokaun A, Büchi FN. J Electrochem Soc 2009;156:B1225–31.
[111] http://www.splusplus.com/, retrieved on February 2010.
[112] St-Pierre J, Jia N, Rahmani R. J Electrochem Soc 2008;155:B315–20.
[113] Kulikovsky AA, Kucemak A, Kornyshev AA. Electrochim Acta 2005;50:1323–33.
[114] Brett DJL, Aguiar P, Brandon NP, Kucernak AR. Int J Hydrogen Energy 2007;32:863–71.
[115] Hartnig C, Manke I, Kardjilov N, Hilger A, Grünerbel M, Kaczerowski J, et al. J Power Sources 2008;176:452–9.
[116] Noponen M, Hottinen T, Mennola T, Mikkola M, Lund P. J Appl Electrochem 2002;32:1081–9.
[117] Hottinen T, Noponen M, Mennola T, Himanen O, Mikkola M, Lund P. J Appl Electrochem 2003;33:265–71.
[118] http://helmbold-messtechnik.de/, retrieved on February 2010.
[119] Santis M, Freunberger SA, Reiner A, Büchi FN. Electrochim Acta 2006;51: 5383–93.
[120] Bender G, Reshetenko TV, Dinh H, Ulsh M, Rocheleau R. ECS Meet Abstr 2008;802:944.
[121] Colinart T, Buchi FN. ECS Meet Abstr 2009;902:1015.


**Luis Carlos Pérez Martínez** is a doctoral candidate at the University of Porto, Faculty of Engineering. He has an undergraduate degree in industrial engineering. Before starting his PhD, he worked in a Mexican alternative energy consultancy firm named Energetic Solutions in Motion S.A. de C.V. trying to develop Clean Development Mechanism (CDM) projects under the Kyoto's Protocol scheme.